PERFORMANCE ANALYSIS OF THE IMPEDANCE BOUNDARY CONDITIONS FOR AXISYMMETRIC EDDY CURRENT PROBLEMS

By
K.A.S.N. Jayasekera

A Thesis
Submitted to the Faculty of Graduate Studies
In Partial Fulfilmant of the Requirement
For the Degree of
Master of Science

Department of Electrical and Computer Engineering
University of Manitoba,
Winnipeg, Manitoba

THE UNIVERSITY OF MANITOBA

FACULTY OF GRADUATE STUDIES

*****

COPYRIGHT PERMISSION

PERFORMANCE ANALYSIS OF THE IMPEDANCE BOUNDARY CONDITIONS FOR AXISYMMETRIC EDDY CURRENT PROBLEMS

BY

K.A.S.N. Jayasekera

A Thesis/Practicum submitted to the Faculty of Graduate Studies of The University of Manitoba in partial fulfillment of the requirement of the degree

Of

MASTER OF SCIENCE

To my parents.

Table of Contents

Appendices

List of Tables

List of Figures

Acknowledgements

I would like to express my deep appreciation and gratitude to Prof. I.R. Ciric for suggesting the thesis topic and for his constant guidance, encouragement and support throughout my research. I thank the members of my thesis examination committee, Prof. Joe LoVetri and Prof. A. Shah, for graciously accepting to review my thesis. Conducting this research work would not have been possible without the financial assistance from Dr. Ciric's research grants and from the University of Manitoba in the form of a Graduate Fellowship. The author would also like to thank his colleagues for their support in many ways and for the stimulating discussions related to the research work. Finally, I would like to thank my parents for their continuous support throughout my academic carrier and for encouraging me to pursue graduate studies.

Winnipeg, Manitoba

October 27, 2003

Nandaka Jayasekera

Abstract

The range of validity of the standard surface impedance and the perfect electric conductor models for the analysis of axisymmetric eddy current problems is thoroughly investigated. These models are used to determine the power losses and the forces acting on conducting objects due to the currents induced by external magnetic fields variable with time. A range of numerical results have been generated for the power losses and the forces for both prolate and oblate spheroidally shaped good conductors and conducting spheres placed in an inducing axisymmetric field.

The numerical results generated for conducting spheroids show the improvement brought by the standard impedance boundary condition with respect to the simpler, perfect electric conductor boundary condition, which is usually employed at higher frequencies. The results obtained using the standard impedance boundary condition are in good agreement with the experimental results available for prolate and oblate conducting spheroids and with the results obtained from the exact analytical solution for conducting spheres, when the skin depth is less than one tenth of the radius of curvature.

Moreover the first order curvature correction for the surface impedance has been also applied for conducting spheroids. Results obtained for the power losses and forces by employing both the standard surface impedance and the perfect conductor boundary conditions are compared with the results obtained by using the impedance boundary condition with first order curvature correction. It is found that the results obtained by using the standard impedance boundary condition are in good agreement with the results obtained with the first order curvature correction for spheroids having the ratio of the depth of penetration to the semi-minor axis less than 1/10.

Chapter 1

Introduction

The analysis of induced currents in solid conducting objects due to the presence of an external quasistationary magnetic field is necessary in numerous areas of applied electromagnetics, such as induction heating, eddy current braking, electromagnetic shielding and electromagnetic levitation.

An accurate study of the induced currents requires the field solution for both the inside and the outside of the conductor. Exact analytical solutions are possible only in a very small number of cases. Numerical solutions require a great deal of computation since the interior of the solid conductor should be discretized using a sufficiently large grid. In order to reduce substantially the amount of computations at high frequencies one can use the simpler perfect electric conductor boundary condition, when only the field solution outside the conductor is needed. On the other hand, more accurate results can be obtained by using the surface impedance boundary condition, when only the field solution in the region external to the conducting object is required. In general, these boundary conditions are called impedance boundary conditions and are categorized as approximate boundary conditions. Various impedance boundary conditions are widely used in numerous areas of applied electromagnetics in order to reduce the complexity of the problem.

1.1 Thesis Outline

In Chapter 1 of this thesis the concept of impedance boundary conditions for solving boundary value problems in applied electromagnetics is summarized. We discuss some of the most widely used impedance boundary conditions such as the standard surface impedance, the perfect electric conductor model, the perfect magnetic conductor boundary conditions and the impedance boundary condition with first order curvature correction. In Chapters 2 & 3 we present in detail the derivation of the analytical solution for the magnetic vector potential for a conducting sphere and a conducting spheroid in the presence of a system of inducing turns by using various impedance boundary conditions. The solutions for the Laplace equation in spherical and spheroidal coordinates are determined by using the method of separation of variables. The constants of integration are determined by applying different impedance boundary conditions.

Chapter 4 contains the derivation of the expressions for the power losses and the forces acting on conducting spheres/spheroids under different boundary conditions. In Chapter 5 of this thesis we present numerical results obtained for the power losses and forces in a normalized form in a way that facilitates the comparison of the performance of different impedance boundary conditions as compared to available experimental results [1] and to results generated using the curvature dependent boundary conditions in the case of conducting spheroids, as well as to numerical results obtained from the exact analytical solution for conducting spheres.

Appendix A provides a simple derivation of the expressions for the surface impedance and the skin depth for a plane wave incident upon a semi-space made of a good conductor. In Appendix B & C some useful properties and relationships for associated Legendre functions and modified Bessel functions, respectively, are given. In Appendix D the expressions for the principal curvatures for both the prolate and oblate shaped spheroids are derived. Appendix E presents a complete derivation of the exact analytical solution for a conducting sphere in

the presence of a system of current-carrying turns.

1.2 Approximate Boundary Conditions

Approximate boundary conditions provide an approximate relationship between the electric and magnetic fields at the interface between two different media, where the properties of the overall medium change discontinuously, which results in discontinuities for some field components. In general, approximate boundary conditions simplify the analytical or numerical solution of field problems involving complex structures. In electromagnetics, approximate boundary conditions are widely used in the analysis of scattering and propagation of waves to simulate the material and geometric properties of surfaces [2]. As an example, let us consider the problem of determining the field scattered by an object immersed in a homogenous medium and illuminated by an electromagnetic field. Knowing the material properties of the object, in principle, it is possible to find the scattered field external to the object by taking in to account the behavior of the fields within the object. This problem can be greatly simplified if the object properties could be simulated via a boundary condition involving only the external fields at the outer surface, thereby converting a two (or more) media problem into a single medium problem. The only requirement for this formulation is that, in the region of interest, the field obtained by using the postulated condition should approximate the actual field to an adequate degree of accuracy [2].

Let us consider an electromagnetic wave incident on the interface between two media (assume both media to be linear, isotropic, homogeneous and source free). At the interface, the electric and magnetic fields satisfy the transition (boundary) conditions [2]

$$[\boldsymbol{n} \times \boldsymbol{E}]_{-}^{+} = -\boldsymbol{J}_{ms} \qquad [\boldsymbol{n} \cdot \mu \boldsymbol{H}]_{-}^{+} = \rho_{ms} \tag{1.1}$$

$$[\boldsymbol{n} \times \boldsymbol{H}]_{-}^{+} = \boldsymbol{J}_{es} \qquad [\boldsymbol{n} \cdot \epsilon \boldsymbol{E}]_{-}^{+} = \rho_{es} \tag{1.2}$$

where $[\ ]^{+}_{-}$ denotes the discontinuity between the [+] and the [−] sides of the interface, $\boldsymbol{n}$ is the unit vector normal to the interface and directed into the [+] side, $\boldsymbol{J}_{es}$ and ρ_{es} are the electric current and the electric charge densities on the surface of discontinuity, respectively, and $\boldsymbol{J}_{ms}$ and ρ_{ms} denote the corresponding magnetic current and magnetic charge densities on the surface of discontinuity, respectively. If the [−] side is a perfect electrical conductor, all the field quantities in this medium are zero by definition and $\boldsymbol{J}_{ms} = \rho_{ms} = 0$. This yields

$$\boldsymbol{n} \times \boldsymbol{E}^{+} = 0 \tag{1.3}$$

$$\boldsymbol{n} \cdot \boldsymbol{H}^{+} = 0 \tag{1.4}$$

Equation (1.3) is referred to as the perfect electric conductor boundary condition (PEC). Conversely, if the [−] side is a perfect magnetic conductor all the field quantities in this medium are zero and $\boldsymbol{J}_{es} = \rho_{es} = 0$. This gives

$$\boldsymbol{n} \times \boldsymbol{H}^{+} = 0 \tag{1.5}$$

$$\boldsymbol{n} \cdot \boldsymbol{E}^{+} = 0 \tag{1.6}$$

Equation (1.5) is the perfect magnetic conductor boundary condition (PMC). Since all the materials are neither perfect electric conductors nor perfect magnetic conductors, the interface cannot support surface currents and therefore the resulting boundary conditions become

$$[\boldsymbol{n} \times \boldsymbol{E}]^{+}_{-} = 0 \qquad [\boldsymbol{n} \times \boldsymbol{H}]^{+}_{-} = 0 \tag{1.7}$$

The above equations show the continuity of the tangential components of the electric and magnetic fields across the interface and are used to find an accurate solution for the field components both inside and outside to the object. However, this involves rigorous solutions

of the field equations as mentioned at the beginning of this chapter.

The simplest approximate boundary conditions are the impedance boundary conditions. They are widely used in applied electromagnetics in order to solve boundary value problems related to electromagnetic scattering, eddy currents and lossy transmission lines. The boundary conditions which assumed a perfect electric or magnetic conductors are the simplest among them. The most widely used impedance boundary condition is the standard impedance boundary condition (SIBC), also called the Leontovich boundary condition, which was developed (1948) for use when the skin depth is relatively small when compared to the dimensions of the object.

Due to the simplicity, ease of use and successful applications, improved or higher order versions of impedance boundary conditions have also been considered for electromagnetic applications. These higher order conditions, often referred to as generalized impedance boundary conditions (GIBC), permit the simulation of more complicated material and composite surfaces with greater accuracy [2]. In the present study, we confined our investigation to the analysis of the performance of the Leontovich boundary conditions for axisymmetric eddy current problems, in which the tangential components of the electric and magnetic field intensities are related via a surface impedance, which is a function of only the electromagnetic properties of the material and the frequency of the field which is incident upon the surface of the object [3].

1.3 Impedance Boundary Conditions

Schelkunoff (1934) first introduced the concept of the surface impedance in electromagnetics for the analysis of coaxial transmission lines and cylindrical shields [4]. For a homogeneous body in which a point on it's surface is defined by an orthogonal curvilinear coordinate system, Rytov (1940) showed that the tangential components of the electric field at the surface could be expressed as series of powers of the depth of penetration of electromagnetic field,

with coefficients that involve the tangential magnetic field components and their tangential derivatives [2]. Leontovich had developed a new form of boundary condition for highly conducting surfaces, which is simpler in the sense of computations [2] i.e.

$$\boldsymbol{n} \times \boldsymbol{E} = Z_s \, \boldsymbol{n} \times [\boldsymbol{n} \times \boldsymbol{H}] \tag{1.8}$$

where $\boldsymbol{n}$ is the outward unit vector normal to the surface, $\boldsymbol{E}$ and $\boldsymbol{H}$ are the electric field and the magnetic field intensities, respectively, at the conductor surface. Z_s is the surface impedance, which is equal to the intrinsic impedance of the medium in which the fields penetrate. In other words, Z_s is the ratio between the tangential components of $\boldsymbol{E}$ and $\boldsymbol{H}$ at the conductor surface. For an isotropic, linear and lossy conducting semi-space, the surface impedance is given by [see Appendix A]

$$Z_s = \sqrt{\frac{\omega\mu}{2\sigma}}(1+j) = \frac{(1+j)}{\delta\sigma} \tag{1.9}$$

where δ is the skin depth for a good conductor,

$$\delta = \sqrt{\frac{2}{\omega\mu\sigma}} \tag{1.10}$$

The validity of the boundary condition (1.8) for surfaces with curvatures requires that [5]

$$|Z_s| \ll Z_0, \qquad \frac{\delta}{R_{min}} \ll 1 \tag{1.11}$$

where Z_0 is the free space wave impedance and R_{min} is the minimum radius of curvature of the surface.

Rytov(1940) developed rigorous derivations of approximate boundary conditions up to the second order, applicable at the curved surfaces of highly conducting bodies [2]. For

geometries with curvature, Leontovich (1948) introduced a first order curvature correction term to the standard surface impedance for small radii of curvatures, whose correct expression is given in [6]. i.e.

$$E_u = (1+p)Z_s H_v \tag{1.12}$$

$$E_v = -(1-p)Z_s H_u \tag{1.13}$$

$$p = \frac{1}{4}(1+j)\delta(K_v - K_u) \tag{1.14}$$

where K_u and K_v are the principal curvatures of the point on the surface corresponding to the principal curvature direction coordinates u and v, respectively, with

$$\boldsymbol{a}_u \times \boldsymbol{a}_v = \boldsymbol{n} \tag{1.15}$$

where $\boldsymbol{n}$ is the unit vector normal to the surface of the conductor and pointing towards the center of curvature, and $\boldsymbol{a}_u$ and $\boldsymbol{a}_v$ are unit vectors along the line of coordinates u and v, respectively, in the directions of increase of the respective coordinates. Since $\boldsymbol{n}$ points into the conductor, the principal curvatures K_u and K_v are considered to be positive wherever the conducting body is convex [6]. In the present study, we have used both the PEC and SIBC, and also the impedance boundary condition with first order curvature correction for deriving analytical expressions for various field quantities.

1.4 Problem Statement

The main objective of the present study is to investigate the performance of impedance boundary conditions, namely, PEC model and the SIBC for the analysis of axisymmetric eddy-current problems. This research work mainly consists of

I. derivation of analytical expressions for the magnetic vector potential produced by a system of circular turns carrying time harmonic currents in the presence of solid conducting spheres/spheroids having a common axis of rotation by using the impedance boundary conditions mentioned above;

II. derivation of the exact analytical solution for the magnetic vector potential produced by a system of circular turns carrying time harmonic currents in the presence of a solid conducting sphere;

III. derivation of expressions for the power losses due to induced currents and the forces acting on conducting spheres and spheroids;

IV. comparison of the numerical results for the power losses and the forces obtained by employing different boundary conditions with the experimental results presented in [1] for conducting spheroids and with the results obtained from the exact analytical solution for spheres;

V. investigation of the performance of the above mentioned boundary conditions for the solution of axisymmetric eddy current problems.

Chapter 2

Analytical Solutions for a Conducting Sphere

Consider a conducting sphere of radius r_0 made of a good conducting material of conductivity σ, placed in an external magnetic field produced by a co-axial circular turn carrying time harmonic current as shown in Fig. 2.1. The system is symmetrical around the z-axis and the spherical coordinates r, θ, φ are used for deriving expressions for various field quantities.

2.1 Determination of the Magnetic Vector Potential Using Impedance Boundary Conditions

Because of the symmetry, the magnetic vector potential $\boldsymbol{A}$ has only a φ-component, $\boldsymbol{A} = \boldsymbol{u}_\varphi A$. Let's assume that outside the sphere $\boldsymbol{A} = \boldsymbol{A}' + \boldsymbol{A}''$, where $\boldsymbol{A}' = \boldsymbol{u}_\varphi A'$ denotes the magnetic vector potential due to the induced currents in the conducting sphere, whereas $\boldsymbol{A}'' = \boldsymbol{u}_\varphi A''$ is the magnetic vector potential produced by the inducing turn alone. $\boldsymbol{A}$ is assumed to satisfy the Coulomb gauge condition $\nabla \cdot \boldsymbol{A} = 0$. $\boldsymbol{A}'$ and $\boldsymbol{A}''$ satisfy the equations [7]

$$\nabla^2 \boldsymbol{A}' = 0 \tag{2.1}$$

$$\nabla^2 \boldsymbol{A}'' = -\mu_0 \boldsymbol{J} \tag{2.2}$$

The electric current density $\boldsymbol{J} = \boldsymbol{u}_\phi J_\phi$ in the filamentary current-carrying turn can be expressed as

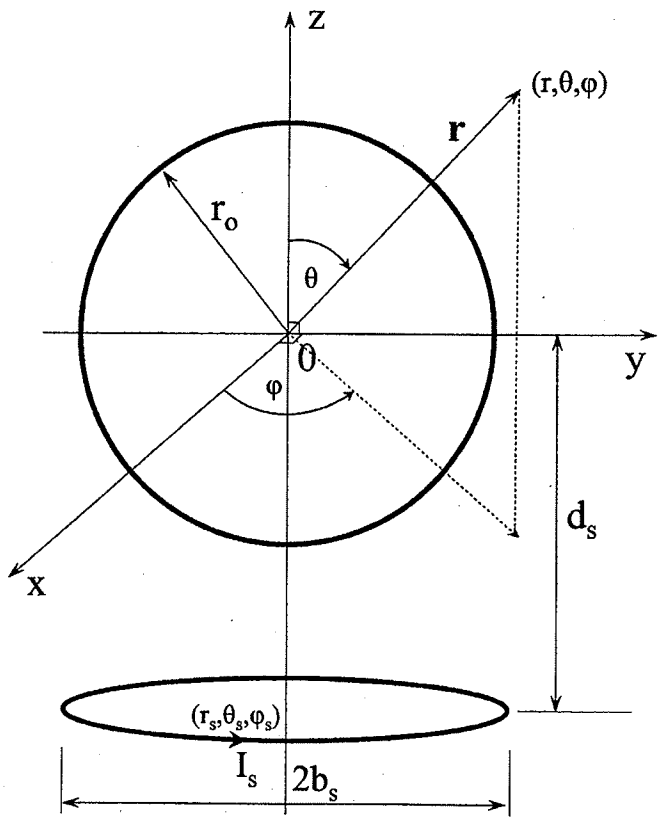

Figure 2.1: Conducting sphere in the presence of a circular current-carrying turn.

$$J_\phi = \frac{I_s \delta(\theta - \theta_s)\delta(r - r_s)}{r} \tag{2.3}$$

where $\delta(\theta - \theta_s)$ and $\delta(r - r_s)$ are one-dimensional Dirac's delta functions, defined by

$$\delta(\tau - \tau_0) = 0 \ , \quad \tau \neq \tau_0$$

$$\int_{-\infty}^{+\infty} \delta(\tau - \tau_0) d\tau = 1$$

$$\int_{-\infty}^{+\infty} f(\tau)\delta(\tau - \tau_0) d\tau = f(\tau_0)$$

where $f(\tau)$ is an arbitrary function continues at τ_0.

2.1.1 Magnetic Vector Potential Due to Induced Currents

A' satisfies the scalar component of the Laplacian of $\boldsymbol{A}'$ in spherical coordinates (see Appendix B).

$$\frac{\partial^2}{\partial r^2}(rA') + \frac{1}{rsin\theta}\frac{\partial}{\partial\theta}\left(sin\theta\frac{\partial}{\partial\theta}A'\right) - \frac{A'}{rsin^2\theta} = 0 \tag{2.4}$$

The solution of (2.4) can be obtained by using the method of separation of variables. Assuming A' to be of the form $A' = L(r)M(\theta)r^{-1}$[8], we get

$$\frac{r^2}{L}\frac{d^2L}{dr^2} + \frac{1}{Msin\theta}\frac{d}{d\theta}\left(sin\theta\frac{dM}{d\theta}\right) - \frac{1}{sin^2\theta} = 0 \tag{2.5}$$

With $\frac{1}{L}r^2\frac{d^2L}{dr^2} = n(n+1)$ we have,

$$\frac{d^2L}{dr^2} - \frac{n(n+1)}{r^2}L = 0 \tag{2.6}$$

whose solution can be written in the form

$$L(r) = \alpha_n r^{n+1} + \beta_n r^{-n} \tag{2.7}$$

where α_n and β_n are constants. Similarly from (2.5) and (2.6) we get

$$\frac{1}{sin\theta}\frac{d}{d\theta}\left(sin\theta\frac{dM}{d\theta}\right) + \left(n(n+1) - \frac{1}{sin^2\theta}\right)M = 0 \tag{2.8}$$

Substituting $x = cos\theta$, (2.8) is brought to the form

$$\frac{d}{dx}\left[(1-x^2)\frac{dM}{dx}\right]+\left[n(n+1)-\frac{1}{1-x^2}\right]M=0 \tag{2.9}$$

The solution of (2.9) is given in Appendix C and can be expressed as

$$M(\theta)=\alpha'_n P_n^1(cos\theta)+\beta'_n Q_n^1(cos\theta) \tag{2.10}$$

where $P_n^1(cos\theta)$ and $Q_n^1(\cos\theta)$ are the associated Legendre functions of the first kind and the second kind, respectively, and α'_n and β'_n are constants. By considering the fact that the magnetic vector potential has a finite value everywhere in the region $r_0 \leq r \leq \infty$, the constant $\alpha_n = 0$ in (2.7). Similarly by considering the properties of the associated Legendre functions as given in Appendix C, and due to the fact that $-1 \leq cos\theta \leq +1$, we have $\beta'_n = 0$. Thus, the magnetic vector potential produced by the induced currents external to the conducting sphere can be expressed as

$$A'=\sum_{n=1}^{\infty} C_n P_n^1(cos\theta) r^{-(n+1)} \tag{2.11}$$

where C_n are constants to be determined.

2.1.2 Magnetic Vector Potential Produced by a Circular Turn Alone

The solution of (2.2) is

$$\boldsymbol{A}''(\boldsymbol{r})=\frac{\mu_0}{4\pi}\int\frac{\boldsymbol{J}(\boldsymbol{r}')}{|\boldsymbol{r}-\boldsymbol{r}'|}d\upsilon' \tag{2.12}$$

where $d\upsilon' = r'^2 sin\theta' dr' d\theta' d\varphi'$. The inverse distance term $1/|\boldsymbol{r}-\boldsymbol{r}'|$ can be expanded as[1]

$$\frac{1}{|\boldsymbol{r}-\boldsymbol{r}'|} = \sum_{n=0}^{\infty}\sum_{m=0}^{\infty}(-1)^m(2-\delta_m)\frac{(n-m)!}{(n+m)!}\frac{r_<^n}{r_>^{n+1}} \cdot P_n^m(cos\theta')P_n^m(cos\theta)cosm(\phi-\phi') \tag{2.13}$$

where $\delta_m = 0$ for $m \neq 0$ and $\delta_m = 1$ for $m = 0$ and $r_<$ and $r_>$ are the smallest and the largest of r and r_s, respectively. The relationship between $\boldsymbol{A}''$ and $\boldsymbol{J}$ is also valid for their scalar components in rectangular coordinates, which are

$$\begin{aligned} J_x &= -J_\phi sin\phi' \qquad & A_x'' &= -A'' sin\phi \\ J_y &= +J_\phi cos\phi' \qquad & A_y'' &= +A'' cos\phi \\ J_z &= 0 \qquad & A_z'' &= 0 \end{aligned} \tag{2.14}$$

Due to the axial symmetry of the field produced by the circular current-carrying turn, the magnitude of $\boldsymbol{A}''$ does not depend on ϕ, thus ϕ can be chosen arbitrarily. Let us consider the semi-plane $\phi = 0$; substituting (2.3) and (2.13) in (2.12) and considering the fact that $\int_0^{2\pi} cos\phi' cos(m\phi')d\phi' = 0$ except for $m = 1$, the magnetic vector potential produced by the circular turn alone can be expressed in the form[8]

$$A'' = \frac{\mu_0 I_s}{2} r_s sin\theta_s \sum_{n=1}^{\infty} \frac{1}{n(n+1)} \frac{r_<^n}{r_>^{n+1}} P_n^1(cos\theta_s)P_n^1(cos\theta) \tag{2.15}$$

The total magnetic vector potential outside the conducting sphere is obtained by superposing the vector potentials produced by the induced currents(A') and the circular turn alone(A'') in the form.

$$A = \sum_{n=1}^{\infty} C_n r^{-(n+1)} P_n^1(cos\theta) + \frac{\mu_0 I_s}{2} sin\theta_s r_s \sum_{n=1}^{\infty} \frac{1}{n(n+1)} \frac{r_<^n}{r_>^{n+1}} P_n^1(cos\theta_s)P_n^1(cos\theta) \tag{2.16}$$

2.1.3 Application of Boundary Conditions

The constants of integration C_n are determined by applying the boundary condition (1.8), which can be simply expressed in terms of the tangential components of the electric and

magnetic field intensities at the conductor surface as

$$Z_s = \left.\frac{E_\varphi}{H_\theta}\right|_{r=r_0} \tag{2.17}$$

From the Maxwell equations for a time harmonic field

$$\nabla \times \boldsymbol{E} = -j\omega \boldsymbol{B} \tag{2.18}$$

Since $\boldsymbol{B} = \nabla \times \boldsymbol{A}$, we get

$$\nabla \times [\boldsymbol{E} + j\omega \boldsymbol{A}] = 0 \tag{2.19}$$

According to the vector identity $\nabla \times \nabla\phi \equiv 0$, (2.19) yields $\boldsymbol{E} = -j\omega \boldsymbol{A} - \nabla\phi$, where ϕ is an electric scalar potential. In what follows, only the induced electric field which is due to the magnetic vector potential is determined, since the electric field due to the scalar potential is normal to the surface of the solid conductor and thus does not appear in the definition of the surface impedance and does not contribute to the losses and the forces exerted upon the conductors. The components of the electric and the magnetic field intensities are expressed in spherical coordinates in the form

$$E_\varphi = -j\omega A \tag{2.20}$$

$$H_\theta = \frac{1}{\mu_0 r}\frac{\partial}{\partial r}(rA) \tag{2.21}$$

$$H_r = -\frac{1}{\mu_0 r sin\theta}\frac{\partial}{\partial \theta}(sin\theta A) \tag{2.22}$$

From (2.17), (2.20) and (2.21) we get

$$\frac{Z_s}{\mu_0}\left\{\sum_{n=1}^{\infty}\left[nC_n r_0^{-(n+2)} - \frac{\mu_0 I_s}{2}\frac{sin\theta_s}{n}\frac{r_0^{n-1}}{r_s^n}P_n^1(cos\theta_s)\right]P_n^1(cos\theta)\right\}$$
$$= -j\omega\left\{\sum_{n=1}^{\infty}\left[C_n r_0^{-(n+1)} + \frac{\mu_0 I_s}{2}\frac{sin\theta_s}{n(n+1)}\frac{r_0^n}{r_s^n}P_n^1(cos\theta_s)\right]P_n^1(cos\theta)\right\} \tag{2.23}$$

By equating the coefficients of $P_n^1(cos\theta)$ in each side of (2.23) we get

$$C_n = \frac{\mu_0 I_s}{2}\frac{sin\theta_s P_n^1(cos\theta_s)}{n(n+1)r_s^n}\left[\frac{Z_s(n+1)r_0^{2n+1} - j\omega\mu_0 r_0^{2(n+1)}}{Z_s n + j\omega\mu_0 r_0}\right] \tag{2.24}$$

Substituting C_n in (2.16) the resultant magnetic vector potential can be expressed as

$$A = \frac{\mu_0 I_s}{2}sin\theta_s\sum_{n=1}^{\infty}\left\{\left[\frac{Z_s(n+1)r_0^{2n+1} - j\omega\mu_0 r_0^{2(n+1)}}{Z_s n + j\omega\mu_0 r_0}\right]\frac{1}{r_s^n r^{n+1}} + r_s\frac{r_<^n}{r_>^{n+1}}\right\}\frac{P_n^1(cos\theta_s)P_n^1(cos\theta)}{n(n+1)} \tag{2.25}$$

Notes

- In the case of an inducing system with N_t number of current-carrying turns in the presence of a conducting sphere having a common axis of rotation, the resultant magnetic vector potential external to the conducting sphere can be obtained by superposing the magnetic vector potentials produced by individual turn.

- It should be remarked that the expressions derived by using the SIBC are also valid for the impedance boundary condition with first order curvature correction as given in (1.12),(1.13) and (1.14) since for a sphere $K_r = K_\theta = 1/r_0$ (see Appendix E).

- In the case of a perfectly conducting sphere, the expressions for the field quantities can be obtained by assuming a zero surface impedance in the corresponding expressions derived for a sphere with a finite conductivity.

Thus for a system with N_t number of inducing turns

$$A = \frac{\mu_0}{2} \sum_{s=1}^{N_t} I_s sin\theta_s \sum_{n=1}^{\infty} \left\{ \left[\frac{Z_s(n+1) r_0^{2n+1} - j\omega\mu_0 r_0^{2(n+1)}}{Z_s n + j\omega\mu_0 r_0} \right] \frac{1}{r_s^n r^{n+1}} + r_s \frac{r_<^n}{r_>^{n+1}} \right\} \frac{P_n^1(cos\theta_s) P_n^1(cos\theta)}{n(n+1)} \tag{2.26}$$

In the case of a perfectly conducting sphere,

$$A = \frac{\mu_0}{2} \sum_{s=1}^{N_t} I_s sin\theta_s \sum_{n=1}^{\infty} \left\{ r_s \frac{r_<^n}{r_>^{n+1}} - \left(\frac{r_0}{r_s}\right)^n \left(\frac{r_0}{r}\right)^{n+1} \right\} \frac{P_n^1(cos\theta_s) P_n^1(cos\theta)}{n(n+1)} \tag{2.27}$$

2.2 The Exact Analytical Solution for a Conducting Sphere

The exact analytical solution for the quasistationary field solutions both internal and external to the conducting sphere in the presence of a system of inducing turns has been already investigated in [9],[10]. The complete derivation for the boundary value problem by considering the continuity of the tangential components of the electric and magnetic field intensities at the interface between the conductor and free space, as in (1.7), is presented in Appendix. F. Thus, the exact analytical solution for the magnetic vector potential both internal and external to the conducting sphere yields

$$A_{in} = \frac{\mu_0}{2} \frac{1}{k r_0^{1/2} r^{1/2}} \sum_{s=1}^{N_t} I_s sin\theta_s \sum_{n=1}^{\infty} \frac{2n+1}{n(n+1)} \left(\frac{r_0}{r_s}\right)^n \frac{j_n(kr)}{j_{n-1}(kr_0)} P_n^1(cos\theta_s) P_n^1(cos\theta), \quad r \le r_0 \tag{2.28}$$

$$A_{ext} = \frac{\mu_0}{2} \sum_{n=1}^{N_t} I_s sin\theta_s \sum_{n=1}^{\infty} \left\{ r_s \frac{r_<^n}{r_>^{n+1}} + \frac{r_0^{2n+1}}{r_s^n r^{n+1}} \left[\frac{(2n+1)}{kr_0} \frac{j_n(kr_0)}{j_{n-1}(kr_0)} - 1 \right] \right\} \cdot \frac{P_n^1(cos\theta_s) P_n^1(cos\theta)}{n(n+1)}, \quad r \ge r_0 \tag{2.29}$$

where $j_n(kr)$ denotes the spherical Bessel functions of the first kind (see Appendix D), $k^2 = j\omega\mu\sigma$ and N_t is the number of inducing turns.

Chapter 3

Analytical Solutions for Conducting Spheroids Using Impedance Boundary Conditions

Let us consider now a conducting spheroid (either prolate or oblate) made of a good conductor and placed in a magnetic field produced by a filamentary circular turn carrying a quasistationary current. The spheroid and the circular turn have the same axis of rotation. Figures 3.1 and 3.2 show the arrangement of the inducing systems with a single current carrying turn in the presence of a conducting prolate and oblate spheroid, respectively. The semi-major and the semi-minor axes in case of a prolate spheroid are a_0 and b_0, respectively, while for an oblate spheroid the semi-major and the semi-minor axes are b_0 and a_0, respectively.

Due to the axial symmetry of the system, the field solutions are independent of φ, which substantially reduces the amount of computations. In section 3.1 we present the derivation of the magnetic vector potential $\boldsymbol{A}$ conditioned by a single inducing turn in the presence of a conducting spheroid. The magnetic vector potential due to a number of inducing turns can be obtained by superposing the magnetic vector potentials produced by individual turns. In order to solve the problem, we used two different orthogonal curvilinear coordinate systems, namely, prolate and oblate spheroidal coordinates for the cases of prolate and oblate spheroids, respectively. The rational for choosing prolate and oblate spheroids for the analysis undertaken is due to the fact that these shapes approximate the geometries of a large variety of real world objects.

3.1 The Choice of Prolate and Oblate Spheroidal Coordinates

Figure 3.1 shows an inducing system having only a single current-carrying turn in the presence of a prolate spheroidal conducting object. The system is axisymmetric and the prolate spheroidal coordinates η, ξ, φ ($-1 \leq \eta \leq +1$, $1 \leq \xi \leq \infty$, and $0 \leq \varphi \leq 2\pi$) are used. The unit vectors $\boldsymbol{u}_\eta$, $\boldsymbol{u}_\xi$ and $\boldsymbol{u}_\varphi$ are as depicted in Fig. 3.1.

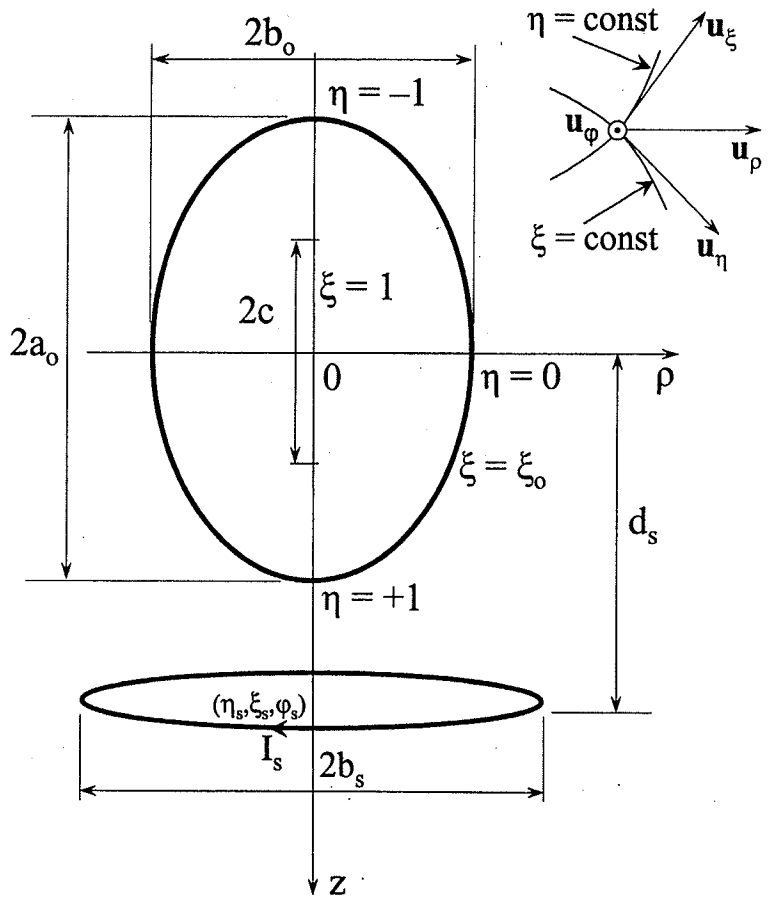

Figure 3.1: Conducting prolate spheroid in the presence of a circular current-carrying turn.

The prolate spheroidal coordinates η, ξ, φ are related to the rectangular cartesien coordinates x, y, z by [1][11]

$$
\begin{aligned}
x &= c[(1-\eta^2)(\xi^2-1)]^{1/2} cos\varphi \\
y &= c[(1-\eta^2)(\xi^2-1)]^{1/2} sin\varphi \\
z &= c\eta\xi
\end{aligned}
\tag{3.1}
$$

The corresponding scale factors h_η, h_ξ and h_φ are [1][11]

$$
\begin{aligned}
h_\eta &= c\left[\frac{\xi^2-\eta^2}{1-\eta^2}\right]^{1/2} \\
h_\xi &= c\left[\frac{\xi^2-\eta^2}{\xi^2-1}\right]^{1/2} \\
h_\varphi &= c[(1-\eta^2)(\xi^2-1)]^{1/2}
\end{aligned}
\tag{3.2}
$$

The lengths of the semi-major axis a_0 and semi-minor axis b_0, the distance to the inducing turn from the origin d_s and the radius of the inducing turn b_s can be expressed in prolate spheroidal coordinates as given in (3.3)[1].

$$
\begin{aligned}
a_0 &= c\xi_0 \ , & b_0 &= c(\xi_0^2-1)^{1/2} \\
d_s &= c\eta_s\xi_s \ , & b_s &= c[(1-\eta_s^2)(\xi_0^2-1)]^{1/2}
\end{aligned}
\tag{3.3}
$$

where η_s,ξ_s denote the coordinates of a point on the circular turn, whereas ξ_0 corresponds to a point on the prolate spheroid whose surface is defined by $\xi = \xi_0 = constant$ $(\xi_s > \xi_0)$. The semi-focal distance of the prolate spheroid c is given by $c = \sqrt{a_0^2 - b_0^2}$.

Figure 3.2 shows the choice of oblate spheroidal coordinates for an oblate spheroidal conducting object in the presence of a single inducing turn. The oblate spheroidal coordinates η, ξ, φ $(-1 \leq \eta \leq +1,\ 0 \leq \xi \leq \infty,\ 0 \leq \varphi \leq 2\pi)$ are related to the rectangular coordinates x, y, z by the following relations [1][11].

$$
\begin{aligned}
x &= c[(1-\eta^2)(\xi^2+1)]^{1/2} cos\varphi \\
y &= c[(1-\eta^2)(\xi^2+1)]^{1/2} sin\varphi \\
z &= c\eta\xi
\end{aligned}
\tag{3.4}
$$

and the corresponding scale factors are

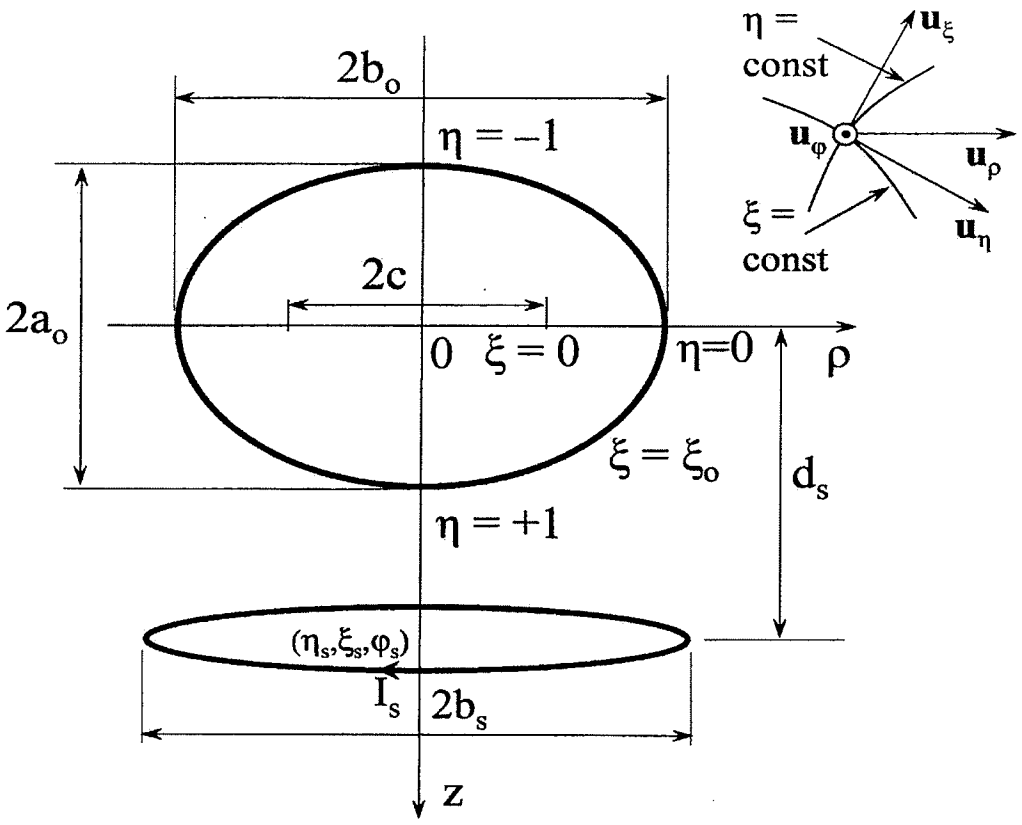

Figure 3.2: Conducting oblate spheroid in the presence of a circular current carrying turn.

$$
\begin{aligned}
h_\eta &= c\left[\frac{\xi^2+\eta^2}{1-\eta^2}\right]^{1/2} \\
h_\xi &= c\left[\frac{\xi^2+\eta^2}{\xi^2+1}\right]^{1/2} \\
h_\varphi &= c[(1-\eta^2)(\xi^2+1)]^{1/2}
\end{aligned}
\tag{3.5}
$$

The semi-focal distance is given by $c = \sqrt{b_0^2 - a_0^2}$.

The lengths a_0, b_0, b_s and the distance d_s in Fig. 3.2 can be expressed as [1]

$$
\begin{aligned}
a_0 &= c\xi_0 \qquad & b_0 &= c(\xi_0^2+1)^{1/2} \\
d_s &= c\eta_s\xi_s \qquad & b_s &= c[(1-\eta_s^2)(\xi_0^2+1)]^{1/2}
\end{aligned}
\tag{3.6}
$$

Note

It is useful to notice that the transformations $\xi \rightarrow j\xi$ and $c \rightarrow -jc$ in the expressions for the physical quantities obtained in prolate spheroidal coordinates give the corresponding expressions in oblate spheroidal coordinates [1]. This transformation will be used whenever we need to derive expressions for various field quantities in oblate spheroidal coordinates from those obtained in prolate spheroidal coordinates.

3.2 Determination of the Magnetic Vector Potential

Let's consider the system shown in Fig. 3.1. Due to the axisymmetry, all field components depend only on η and ξ. The magnetic vector potential $\boldsymbol{A}$ has only a φ-component, $\boldsymbol{A} = \boldsymbol{u}_\varphi A$, and can be determined outside the spheroid in the form

$$\boldsymbol{A} = \boldsymbol{A}'(\eta, \xi) + \boldsymbol{A}''(\eta, \xi) \tag{3.7}$$

where $\boldsymbol{A}' = \boldsymbol{u}_\varphi A'$ is the magnetic vector potential due to the induced currents in the conducting spheroid and $\boldsymbol{A}'' = \boldsymbol{u}_\varphi A''$ is the magnetic vector potential produced by the circular turn alone. $\boldsymbol{A}$ is assumed to be satisfy the Coulomb gauge condition $\nabla \cdot \boldsymbol{A} = 0$. $\boldsymbol{A}'$ and $\boldsymbol{A}''$ satisfy the equations [7]

$$\nabla^2 \boldsymbol{A}' = 0 \tag{3.8}$$

$$\nabla^2 \boldsymbol{A}'' = -\mu_0 \boldsymbol{J} \tag{3.9}$$

where $\boldsymbol{J}$ is the conduction current density, which has only an azimuthal component $\boldsymbol{J} = \boldsymbol{u}_\varphi J_\varphi$, corresponding to the filamentary current-carrying conductor and can be expressed as

$$\begin{aligned} J_\varphi &= \frac{i_s \delta(\eta - \eta_s)\delta(\xi - \xi_s)}{(h_\eta h_\xi)_{\eta_s, \xi_s}} \\ &= \frac{i_s[(1-\eta_s^2)(\xi_s^2 - 1)]^{1/2}\delta(\eta - \eta_s)\delta(\xi - \xi_s)}{c^2(\xi_s^2 - \eta_s^2)} \end{aligned} \tag{3.10}$$

where $\delta(\eta-\eta_s)$ and $\delta(\xi-\xi_s)$ are the one dimensional Dirac delta functions.

Equation (3.8) becomes (see Appendix B)

$$\frac{1}{c^2(\xi^2-\eta^2)}\Big\{(1-\eta^2)^{1/2}\frac{\partial^2}{\partial\eta^2}[(1-\eta^2)^{1/2}A'] + (\xi^2-1)^{1/2}\frac{\partial^2}{\partial\xi^2}[(\xi^2-1)^{1/2}A']\Big\} = 0 \qquad (3.11)$$

The corresponding equation for (3.11) in oblate spheroidal coordinates can be obtained simply by using the transformation $\xi \to j\xi, c \to -jc$,

$$\frac{1}{c^2(\xi^2+\eta^2)}\Big\{(1-\eta^2)^{1/2}\frac{\partial^2}{\partial\eta^2}[(1-\eta^2)^{1/2}A'] + (\xi^2+1)^{1/2}\frac{\partial^2}{\partial\xi^2}[(\xi^2+1)^{1/2}A']\Big\} = 0 \qquad (3.12)$$

3.2.1 Magnetic Vector Potential Due to Induced Currents

Equation (3.11) and (3.12) can be solved by using the method of separation of variables. Let us assume that the solution of (3.11) can be expressed in the form

$$A'(\eta,\xi) = L(\eta)M(\xi) \qquad (3.13)$$

Substituting (3.13) in (3.11) and dividing by $L(\eta)M(\xi)$, yields

$$\frac{1}{L(\eta)}\frac{d}{d\eta}\Big[(1-\eta^2)\frac{d}{d\eta}L(\eta)\Big] - \frac{1}{1-\eta^2} + \frac{1}{M(\xi)}\frac{d}{d\xi}\Big[(\xi^2-1)\frac{d}{d\xi}M(\xi)\Big] + \frac{1}{1-\xi^2} = 0 \qquad (3.14)$$

Taking the separation constant in the form $n(n+1)$ with n being an integer gives

$$\frac{1}{L(\eta)}\frac{d}{d\eta}\Big[(1-\eta^2)\frac{d}{d\eta}L(\eta)\Big] - \frac{1}{1-\eta^2} = -n(n+1) \qquad (3.15)$$

i.e.

$$\frac{d}{d\eta}\Big[(1-\eta^2)\frac{d}{d\eta}L(\eta)\Big]+\Big[n(n+1)-\frac{1}{1-\eta^2}\Big]L(\eta)=0 \tag{3.16}$$

Equation (3.16) is in the form of (C.3) in Appendix C and its solution can be expressed in terms of associated Legendre functions of the first kind P_n^1 and the second kind Q_n^1 in the form

$$L(\eta)=\alpha_n P_n^1(\eta)+\beta_n Q_n^1(\eta) \tag{3.17}$$

Similarly we have,

$$M(\xi)=\alpha_n' P_n^1(\xi)+\beta_n' Q_n^1(\xi) \tag{3.18}$$

$\alpha_n, \alpha_n', \beta_n$ and β_n' are constants of integration. Due to the fact that $1 \leq \xi \leq \infty$ and $-1 \leq \eta \leq +1$ in case of a prolate spheroid, and by considering the properties of associated Legendre functions as given in (C.11) in Appendix C, the solution for (3.14) is expressed in the form

$$A'=\sum_{n=1}^{\infty} C_n Q_n^1(\xi) P_n^1(\eta) \tag{3.19}$$

where C_n are constants to be determined.

3.2.2 Magnetic Vector Potential Produced by a Circular Turn Alone

The solution of (3.9) can be expressed as

$$\boldsymbol{A}''(\boldsymbol{r})=\frac{\mu_0}{4\pi}\int \frac{\boldsymbol{J}(\boldsymbol{r}')}{|\boldsymbol{r}-\boldsymbol{r}'|}d\upsilon' \tag{3.20}$$

where $\boldsymbol{r}$ is the position vector of the observation point and $\boldsymbol{r}'$ is the position vector of the source point. The inverse distance $1/|\boldsymbol{r}-\boldsymbol{r}'|$ can be expanded in terms of prolate spheroidal

harmonics [1].

$$\begin{aligned}\frac{1}{|\boldsymbol{r}-\boldsymbol{r}'|} =& \frac{1}{c}\sum_{n=0}^{\infty}\sum_{m=0}^{\infty}(-1)^m(2-\delta_m)(2n+1)\left[\frac{(n-m)!}{(n+m)!}\right]^2 \\ & \cdot P_n^m(\xi_<)Q_n^m(\xi_>)P_n^m(\eta')P_n^m(\eta)cosm(\varphi-\varphi')\end{aligned} \tag{3.21}$$

The quantity δ_m has the value $\delta_m = 0$ for $m \neq 0$ and $\delta_m = 1$ for $m = 0$, whereas $\xi_<$ and $\xi_>$ are the smallest and greatest of ξ and ξ_s, respectively. The relationship between $\boldsymbol{A}''$ and $\boldsymbol{J}$ is also valid for their scalar components in rectangular coordinates, i.e.

$$\begin{aligned} J_x &= -J_\varphi sin\varphi' \qquad & A_x &= -A'' sin\varphi \\ J_y &= +J_\varphi cos\varphi' \qquad & A_y &= +A'' cos\varphi \\ J_z &= 0 \qquad & A_z &= 0 \end{aligned} \tag{3.22}$$

Due to the axial symmetry of the system, the magnitude of $\boldsymbol{A}''$ does not depend on φ. For convenience, let us consider the semi-plane which is defined by $\varphi = 0$. With $dv' = h_{\eta'}h_{\xi'}h_{\varphi'}d\xi'd\eta'd\varphi'$ and substituting (3.21) and (3.10) in (3.20), A'' can be expressed in the form

$$\begin{aligned}A'' =& \frac{\mu_0 I_s}{4\pi}\frac{[(1-\eta_s^2)(\xi_s^2-1)]^{1/2}}{(\xi_s^2-\eta_s^2)}\sum_{n=0}^{\infty}\sum_{m=0}^{\infty}(-1)^m(2-\delta_m)(2n+1)\left[\frac{(n-m)!}{(n+m)!}\right]^2 \\ & \cdot P_n^m(\eta)\int_v \delta(\eta'-\eta_s)\delta(\xi'-\xi_s)(\xi'^2-\eta'^2)P_n^m(\xi_<)Q_n^m(\xi_>) \\ & \cdot P_n^m(\eta')cos\varphi' cos(m\varphi')d\eta'd\xi'd\varphi'\end{aligned} \tag{3.23}$$

Due to the fact that $\int_0^{2\pi} cos\varphi' cos(m\varphi')d\varphi' = 0$ except for $m = 1$ in (3.23), A'' can finally be expressed in the form

$$A'' = \frac{-\mu_0 I_s}{2}[(1-\eta_s^2)(\xi_s^2-1)]^{1/2}\sum_{n=1}^{\infty}\frac{2n+1}{[n(n+1)]^2}P_n^1(\xi_<)Q_n^1(\xi_>)P_n^1(\eta_s)P_n^1(\eta) \tag{3.24}$$

In the case of an oblate spheroid, the expressions for A'' can be deduced from (3.24) in the form

$$A'' = \frac{-j\mu_0 i_s}{2}[(1-\eta_s^2)(\xi_s^2+1)]^{1/2}\sum_{n=1}^{\infty}\frac{2n+1}{[n(n+1)]^2}P_n^1(j\xi_<)Q_n^1(j\xi_>)P_n^1(\eta_s)P_n^1(\eta) \tag{3.25}$$

3.2.3 Application of Boundary Conditions

From (3.7),(3.19) and (3.24), the total magnetic vector potential external to a prolate spheroid can be expressed as

$$\begin{aligned} A = \sum_{n=1}^{\infty}\Big\{ & C_n Q_n^1(\xi)P_n^1(\eta) - \frac{\mu_0 I_s}{2}[(1-\eta_s^2)(\xi_s^2-1)]^{1/2} \\ & \cdot \frac{(2n+1)}{[n(n+1)]^2}P_n^1(\xi_<)Q_n^1(\xi_>)P_n^1(\eta_s)P_n^1(\eta)\Big\} \end{aligned} \tag{3.26}$$

In the case of an oblate spheroid, the expression for A becomes

$$\begin{aligned} A = \sum_{n=1}^{\infty}\Big\{ & C_n Q_n^1(j\xi)P_n^1(\eta) - \frac{j\mu_0 I_s}{2}[(1-\eta_s^2)(\xi_s^2+1)]^{1/2} \\ & \cdot \frac{(2n+1)}{[n(n+1)]^2}P_n^1(j\xi_<)Q_n^1(j\xi_>)P_n^1(\eta_s)P_n^1(\eta)\Big\} \end{aligned} \tag{3.27}$$

The constants C_n in (3.26) are determined by applying the SIBC as given in (1.8), which can be expressed in terms of the tangential components of the electric and magnetic fields at the conductor surface in the form.

$$-\frac{E_\varphi}{H_\eta}\bigg|_{\xi=\xi_0} = Z_s \tag{3.28}$$

The components of the magnetic field densities B_η and B_ξ are obtained in prolate spheroidal coordinates from, $\boldsymbol{B} = \nabla \times \boldsymbol{A}$ in the form

$$\begin{aligned} B_\eta &= \frac{1}{h_\xi h_\varphi}\frac{\partial}{\partial \xi}(h_\xi A) \\ B_\xi &= \frac{-1}{h_\eta h_\varphi}\frac{\partial}{\partial \eta}(h_\eta A) \end{aligned} \tag{3.29}$$

By substituting the corresponding scale factors in prolate spheroidal coordinates, (3.29) can

be written as

$$B_\eta = \frac{1}{c}\frac{1}{(\xi^2-\eta^2)^{1/2}}\frac{\partial}{\partial\xi}\left[(\xi^2-1)^{1/2}A\right] \tag{3.30}$$

$$B_\xi = \frac{-1}{c}\frac{1}{(\xi^2-\eta^2)^{1/2}}\frac{\partial}{\partial\eta}\left[(1-\eta^2)^{1/2}A\right] \tag{3.31}$$

E has a single component E_φ such that

$$E_\varphi = -j\omega A \tag{3.32}$$

Constants of integration in prolate spheroidal coordinates

The magnetic field intensity H_η at the conductor surface, $\xi = \xi_0$ is determined in the case of a prolate conducting spheroid from (3.30)and (3.26), and can be expressed as

$$\begin{aligned} H_\eta\Big|_{\xi=\xi_0} = &\frac{1}{c\mu_0\sqrt{\xi_0^2-\eta^2}}\sum_{n=1}^{\infty}\Big\{C_n n(n+1)Q_n(\xi_0) - \frac{\mu_0 I_s}{2}[(1-\eta_s^2)(\xi_s^2-1)]^{1/2} \\ &\cdot\frac{(2n+1)}{n(n+1)}P_n(\xi_0)Q_n^1(\xi_s)P_n^1(\eta_s)\Big\}P_n^1(\eta) \end{aligned} \tag{3.33}$$

The properties of the associated Legendre functions given in (C.7) in Appendix C were used in the above computations, and P_n and Q_n are the Legendre functions of the first kind and the second kind, respectively. The electric field intensity E_φ at the conductor surface can be obtained from (3.32), with A as given in (3.26), in the form

$$\begin{aligned} E_\varphi\Big|_{\xi=\xi_0} = &-j\omega\sum_{n=1}^{\infty}\Big\{C_n Q_n^1(\xi_0)P_n^1(\eta) - \frac{\mu_0 I_s}{2}[(1-\eta_s^2)(\xi_s^2-1)]^{1/2} \\ &\cdot\frac{(2n+1)}{[n(n+1)]^2}P_n^1(\xi_0)Q_n^1(\xi_s)P_n^1(\eta_s)P_n^1(\eta)\Big\} \end{aligned} \tag{3.34}$$

By substituting $E_\varphi\big|_{\xi=\xi_0}$ and $H_\eta\big|_{\xi=\xi_0}$ in (3.28) we get

$$\sum_{n=1}^{\infty} j\omega\Big\{C_n Q_n^1(\xi_0) - \frac{\mu_0 I_s}{2}[(1-\eta_s^2)(\xi_s^2-1)]^{1/2}\frac{(2n+1)}{[n(n+1)]^2}P_n^1(\xi_0)Q_n^1(\xi_s)$$
$$\cdot P_n^1(\eta_s)\Big\}P_n^1(\eta) = \frac{Z_s}{c\sqrt{\xi_0^2-\eta^2}}\sum_{n=1}^{\infty}\Big\{\frac{C_n}{\mu_0}n(n+1)Q_n(\xi_0) - \frac{I_s}{2}[(1-\eta_s^2)(\xi_s^2-1)]^{1/2} \tag{3.35}$$
$$\cdot\frac{(2n+1)}{n(n+1)}P_n(\xi_0)Q_n^1(\xi_s)P_n^1(\eta_s)\Big\}P_n^1(\eta)$$

The left hand side of (3.35) is of the form

$$\sum_{n=1}^{\infty}\{C_n\lambda_n - I_s\chi_n\}P_n^1(\eta) \tag{3.36}$$

and the right hand side can be written as

$$\sum_{n=1}^{\infty}\{C_n\alpha_n - I_s\beta_n\}\frac{P_n^1(\eta)}{\sqrt{\xi_0^2-\eta^2}} \tag{3.37}$$

where $\lambda_n, \chi_n, \alpha_n$ and β_n are independent of η,

$$\begin{aligned}
\lambda_n =& j\omega Q_n^1(\xi_0)\\
\chi_n =& \frac{j\omega\mu_0}{2}[(1-\eta_s^2)(\xi_s^2-1)]^{1/2}\frac{(2n+1)}{[n(n+1)]^2}P_n^1(\xi_0)Q_n^1(\xi_s)P_n^1(\eta_s)\\
\alpha_n =& \frac{Z_s}{c\mu_0}n(n+1)Q_n(\xi_0)\\
\beta_n =& \frac{Z_s}{2c}[(1-\eta_s^2)(\xi_s^2-1)]^{1/2}\frac{(2n+1)}{n(n+1)}P_n(\xi_0)Q_n^1(\xi_s)P_n^1(\eta_s)
\end{aligned} \tag{3.38}$$

Let us assume that we can find a constant k_n such that (3.37) can be expressed as a summation of an infinite series of $k_n P_n^1(\eta)$ in the form

$$\sum_{n=1}^{\infty}\{C_n\alpha_n - I_s\beta_n\}\frac{P_n^1(\eta)}{\sqrt{\xi_0^2-\eta^2}} = \sum_{n=1}^{\infty}k_n P_n^1(\eta) \tag{3.39}$$

Thus (3.35) can be expressed in the form

$$\sum_{n=1}^{\infty}\{C_n\lambda_n - I_s\chi_n\}P_n^1(\eta) = \sum_{n=1}^{\infty} k_n P_n^1(\eta) \tag{3.40}$$

Multiplying (3.39) by $P_m^1(\eta)$ and integrating with respect to η $(-1 \leq \eta \leq +1)$ we get

$$\sum_{n=1}^{\infty}\Big\{C_n\alpha_n - I_s\beta_n\Big\}\int_{-1}^{+1}\frac{P_n^1(\eta)P_m^1(\eta)}{\sqrt{\xi_0^2-\eta^2}}d\eta = \sum_{n=1}^{\infty} k_n\int_{-1}^{+1} P_n^1(\eta)P_m^1(\eta)d\eta \tag{3.41}$$

Using the orthogonality property of associated Legendre functions as given in (C.10) in Appendix C, the integral in the right hand side of the above equation can be evaluated, as

$$\int_{-1}^{+1} P_n^1(\eta)P_m^1(x)d\eta = \begin{cases} \frac{2m(m+1)}{2m+1} & \text{if } n = m, \\ 0 & \text{if } n \neq m. \end{cases} \tag{3.42}$$

From (3.41) and (3.42) we get

$$k_m = \frac{2m+1}{2m(m+1)}\sum_{n=1}^{\infty}\Big\{C_n\alpha_n M_{nm} - I_s\beta_n M_{nm}\Big\} \tag{3.43}$$

in which

$$M_{nm} = \int_{-1}^{+1}\frac{P_n^1(\eta)P_m^1(\eta)}{\sqrt{\xi_0^2-\eta^2}}d\eta. \tag{3.44}$$

Substituting k_m from (3.43) in (3.40), we get

$$C_m\lambda_m - I_s\chi_m = \frac{2m+1}{2m(m+1)}\sum_{n=1}^{\infty}\Big\{C_n\alpha_n M_{nm} - I_s\beta_n M_{nm}\Big\} \tag{3.45}$$

Truncating the infinite series in (3.45) at $n = N$ gives a system of N linear equations with N unknowns for the constants C_n. In matrix form this system can be expressed as

$$\Big[\ \mathrm{C}\ \Big]_{N\times 1} = I_s \Big[\mathrm{G}\Big]^{-1}_{N\times N} \Big[\mathrm{D}\Big]_{N\times 1} \tag{3.46}$$

where

$$\begin{aligned} g_{mn} &= \begin{cases} \alpha_n M_{mn} \frac{2m+1}{2m(m+1)} & \text{for } n \neq m, \\ \alpha_n M_{mm} \frac{2m+1}{2m(m+1)} - \lambda_m & \text{for } n = m. \end{cases} \\ d_m &= \frac{2m+1}{2m(m+1)} \sum_{n=1}^{\infty} \Big\{ \beta_n M_{mn} - \chi_m \Big\} \end{aligned} \tag{3.47}$$

Constants of integration in oblate spheroidal coordinates

In case of an oblate spheroid the magnetic field intensity H_η and the electric field intensity E_φ at the conductor surface can be obtained from (3.33) and (3.34), respectively, by using the transformation $\xi \rightarrow j\xi$ and $c \rightarrow -jc$, in the form

$$\begin{aligned} H_\eta\Big|_{\xi=\xi_0} =& \frac{1}{c\mu_0\sqrt{\xi_0^2+\eta^2}} \sum_{n=1}^{\infty} \Big\{ C_n n(n+1) Q_n(j\xi_0) - \frac{j\mu_0 I_s}{2} [(1-\eta_s^2)(\xi_s^2+1)]^{1/2} \\ & \cdot \frac{(2n+1)}{n(n+1)} P_n(j\xi_0) Q_n^1(j\xi_s) P_n^1(\eta_s) \Big\} P_n^1(\eta) \end{aligned} \tag{3.48}$$

$$\begin{aligned} E_\varphi\Big|_{\xi=\xi_0} =& -j\omega \sum_{n=1}^{\infty} \Big\{ C_n Q_n^1(j\xi_0) P_n^1(\eta) - \frac{j\mu_0 I_s}{2} [(1-\eta_s^2)(\xi_s^2+1)]^{1/2} \\ & \cdot \frac{(2n+1)}{[n(n+1)]^2} P_n^1(j\xi_0) Q_n^1(j\xi_s) P_n^1(\eta_s) P_n^1(\eta) \Big\} \end{aligned} \tag{3.49}$$

Substituting $H_\eta\big|_{\xi=\xi_0}$ and $E_\varphi\big|_{\xi=\xi_0}$ in (3.28) yields an equation of the form

$$\sum_{n=1}^{\infty} \Big\{ C_n \lambda_n' + I_s \chi_n' \Big\} P_n^1(\eta) = \sum_{n=1}^{\infty} \{ C_n \alpha_n' - I_s \beta_n' \} \frac{P_n^1(\eta)}{\sqrt{\xi_0^2+\eta^2}} \tag{3.50}$$

where $\lambda_n', \chi_n', \alpha_n'$ and β_n' are independent of η

$$
\begin{aligned}
\lambda'_n =& j\omega Q_n^1(j\xi_0) \\
\chi'_n =& \frac{\omega\mu_0}{2}[(1-\eta_s^2)(\xi_s^2+1)]^{1/2}\frac{(2n+1)}{[n(n+1)]^2}P_n^1(j\xi_0)Q_n^1(j\xi_s)P_n^1(\eta_s) \\
\alpha'_n =& \frac{Z_s}{c\mu_0}n(n+1)Q_n(j\xi_0) \\
\beta'_n =& \frac{jZ_s}{2c}[(1-\eta_s^2)(\xi_s^2+1)]^{1/2}\frac{(2n+1)}{n(n+1)}P_n(j\xi_0)Q_n^1(j\xi_s)P_n^1(\eta_s)
\end{aligned}
\tag{3.51}
$$

Assuming that the right hand side of (3.50) can be expressed in the form

$$
\sum_{n=1}^{\infty}\{C_n\alpha'_n - I_s\beta'_n\}\frac{P_n^1(\eta)}{\sqrt{\xi_0^2+\eta^2}} = \sum_{n=1}^{\infty}k'_nP_n^1(\eta) \tag{3.52}
$$

where k'_n is independent on η, and employing the same technique to determine k'_m in (3.52) as in the case of k_m yields finally

$$
k'_m = \frac{2m+1}{2m(m+1)}\sum_{n=1}^{\infty}\Big\{C_n\alpha'_nM'_{nm} - I_s\beta'_nM'_{nm}\Big\} \tag{3.53}
$$

in which

$$
M'_{nm} = \int_{-1}^{+1}\frac{P_n^1(\eta)P_m^1(\eta)}{\sqrt{\xi_0^2+\eta^2}}d\eta. \tag{3.54}
$$

From (3.50),(3.52) and (3.53) when $n=m$, we get

$$
C_m\lambda'_m + I_s\chi'_m = \frac{2m+1}{2m(m+1)}\sum_{n=1}^{\infty}\Big\{C_n\alpha'_nM'_{nm} - I_s\beta'_nM'_{nm}\Big\} \tag{3.55}
$$

By truncating the infinite series in (3.55) at $n=N$, a system of N linear equations with N unknowns is obtained for the constants of integration C_m, which can be written in matrix form

$$
\Big[\ \mathrm{C}\ \Big]_{N\times 1} = I_s\Big[\mathrm{G}'\Big]^{-1}_{N\times N}\Big[\mathrm{D}'\Big]_{N\times 1} \tag{3.56}
$$

where

$$g'_{mn} = \begin{cases} \alpha'_n M'_{mn} \frac{2m+1}{2m(m+1)} & \text{for } n \neq m, \\ \alpha'_n M'_{mm} \frac{2m+1}{2m(m+1)} - \lambda_m & \text{for } n = m. \end{cases}$$
$$d'_m = \frac{2m+1}{2m(m+1)} \sum_{n=1}^{\infty} \left\{ \beta'_n M'_{mn} + \chi'_m \right\} \tag{3.57}$$

Determination of C_n with first order curvature correction

An improved solution to the eddy-current problem is obtained by applying the impedance boundary condition with first order curvature correction, as described in section 1.3. Consider a good conductor in the form of a prolate spheroid, as depicted in Fig. 3.1. The principal curvatures K_φ and K_η are defined in (E.4) and (E.7) in Appendix E. Since $\boldsymbol{u}_\eta \times \boldsymbol{u}_\varphi = \boldsymbol{n}$, in which $\boldsymbol{n}$ is the unit vector normal to the surface and pointed towards the center of the curvature (see Fig. E.1 in Appendix E), from (1.12),(1.13) and (1.15) select $K_u = K_\eta$ and $K_v = K_\varphi$. Thus, the curvature dependent boundary condition for the tangential components E_φ and H_η at the conductor surface can be expressed as

$$-\left.\frac{E_\varphi}{H_\eta}\right|_{\xi=\xi_0} = Z'_s = (1-p)Z_s \tag{3.58}$$

where $p = \frac{1}{4}(1+j)\delta(K_\varphi - K_\eta)$ and the depth of penetration δ is given by (A.16). The constants of integration C_n are determined in the same way as in the case of the SIBC, with Z_s replaced by the corrected surface impedance Z'_s in (3.28). In the case of an oblate spheroid the principal curvatures are defined in (E.8) and (E.9) in Appendix E and the same procedure can be employed to determine the constants of integration.

3.3 Special Case: Perfect Conductor Model

For a perfectly conducting spheroid in the presence of a circular turn carrying time harmonic current the constants of integration can be obtained by taking a zero surface impedance in (3.35). This yields

$$C_n = \frac{\mu_0 I_s}{2}\left[(1-\eta_s^2)(\xi_s^2-1)\right]^{1/2}\frac{(2n+1)}{[n(n+1)]^2}\frac{P_n^1(\xi_0)}{Q_n^1(\xi_0)}Q_n^1(\xi_s)P_n^1(\eta_s) \tag{3.59}$$

Thus the magnetic vector potential external to a perfectly conducting prolate spheroid can be determined in the form [1]

$$\begin{aligned} A_\varphi(\eta,\xi) =& \frac{\mu_0 I_s}{2}\left[(1-\eta_s^2)(\xi_s^2-1)\right]^{1/2}\sum_{n=1}^{\infty}\frac{(2n+1)}{[n(n+1)]^2}\left[\frac{P_n^1(\xi_0)}{Q_n^1(\xi_0)}Q_n^1(\xi_s)Q_n^1(\xi)\right. \\ & \left. - P_n^1(\xi_<)Q_n^1(\xi_>)\right]P_n^1(\eta_s)P_n^1(\eta) \end{aligned} \tag{3.60}$$

and for an oblate spheroid in the form

$$\begin{aligned} A_\varphi(\eta,\xi) =& \frac{j\mu_0 i_s}{2}\left[(1-\eta_s^2)(\xi_s^2+1)\right]^{1/2}\sum_{n=1}^{\infty}\frac{(2n+1)}{[n(n+1)]^2}\left[\frac{P_n^1(j\xi_0)}{Q_n^1(j\xi_0)}Q_n^1(j\xi_s)Q_n^1(j\xi)\right. \\ & \left. - P_n^1(j\xi_<)Q_n^1(j\xi_>)\right]P_n^1(\eta_s)P_n^1(\eta) \end{aligned} \tag{3.61}$$

The resultant magnetic vector potential produced by a perfectly conducting sphere in the presence of a circular turn carrying time harmonic current can be deduced from the expression derived for a perfectly conducting prolate spheroid by performing the following transformations to spherical coordinates(r,θ) [1].

$$\begin{gathered} c \to 0;\ \ \xi_0, \xi_s, \xi \to \infty;\ \ \eta_s \to cos\theta_s;\ \ \eta \to cos\theta; \\ c\xi_0 \to r_0;\ \ c\xi_s \to r_s;\ \ c\xi \to r \end{gathered} \tag{3.62}$$

The asymptotic expansions of associated Legendre functions given in (C.12) in Appendix C are employed to obtained the resultant magnetic vector potential in the form

$$A = \frac{\mu_0}{2} I_s sin\theta_s \sum_{n=1}^{\infty} \left\{ r_s \frac{r_<^n}{r_>^{n+1}} - \left(\frac{r_0}{r_s}\right)^n \left(\frac{r_0}{r}\right)^{n+1} \right\} \frac{P_n^1(cos\theta_s) P_n^1(cos\theta)}{n(n+1)} \tag{3.63}$$

where r_0 is the radius of the sphere, and $r_<$ and $r_>$ are the smallest and the greatest of r and r_s, respectively, in which (r_s, θ_s) defines a point on the filamentary current-carrying conductor.

Magnetic vector potential produced by an inducing system with N number of turns

For an inducing system consists of N coaxial filamentary inducing turns, carrying time harmonic currents, the resultant magnetic vector potential produced in the presence of the solid induced conductor is determined by the superposition of the magnetic vector potentials produced by the individual turns acting separately.

Chapter 4

Power Losses and Forces for Conducting Spheres and Spheroids

4.1 Active Power Loss Due to Induced Currents

The losses due to the induced currents in solid conducting bodies can be computed approximately if either the tangential component of the magnetic field intensity or the tangential component of the electric field intensity is known. Assuming the induced currents to be distributed over the surface of the body, the active power dissipated in it can be expressed as

$$P = \frac{1}{2} \oint_s R_s \, |\boldsymbol{J}_s|^2 \, ds \tag{4.1}$$

where R_s is the surface resistance of a good conductor (see Appendix A) and $\boldsymbol{J}_s$ is the surface density of the currents induced,

$$\boldsymbol{J}_s = \boldsymbol{n} \times \boldsymbol{H}\big|_s \tag{4.2}$$

Thus, (4.1) can be expressed in terms of the tangential component of the magnetic field intensity H_t on the conductor surface in the form

$$P = \frac{1}{2} \oint_s R_s \, |\boldsymbol{H}_t|^2 \, ds \tag{4.3}$$

where the integration is performed over the surface of the conducting object.

4.1.1 Losses in Conducting Spheres

From (4.3) the power loss in a conducting sphere can be expressed as

$$P = \pi r_0^2 R_s \int_0^{\pi} |H_\theta|^2_{r=r_0} \, sin\theta d\theta \tag{4.4}$$

for both the perfect conductor and the surface impedance models, where R_s is the surface resistance as defined in Appendix A. For the surface impedance model the magnetic field intensity H_θ at the conductor surface is determined from (2.21) with A as given in (2.25),

$$H_\theta\Big|_{r=r_0} = \frac{I_s}{2} sin\theta_s \sum_{n=1}^{\infty} \frac{1}{\left(1 + \frac{Z_s n}{j\omega\mu_0 r_0}\right)} \frac{2n+1}{n(n+1)} \frac{r_0^{n-1}}{r_s^n} P_n^1(cos\theta_s) P_n^1(cos\theta) \tag{4.5}$$

Substituting H_θ in (4.4) and using the orthogonality property of the associated Legendre functions as given in (C.10) in Appendix C, the power loss in a conducting sphere in the presence of a single inducing turn can be expressed as

$$P = \frac{\pi R_s I_s^2}{2} sin^2\theta_s \sum_{n=1}^{\infty} \frac{2n+1}{n(n+1)} \left[\left(\frac{r_0}{r_s}\right)^n \frac{P_n^1(cos\theta_s)}{\sqrt{(1+\mathcal{R})^2 + \mathcal{R}^2}} \right]^2 \tag{4.6}$$

where $\mathcal{R} \equiv R_s n / \omega\mu_0 r_0$. For an inducing system with N_t number of current carrying turns, the resultant power loss is given by

$$P = \frac{\pi R_s}{2} \sum_{n=1}^{\infty} \frac{2n+1}{n(n+1)} \left[\sum_{s=1}^{N_t} I_s sin\theta_s \left(\frac{r_0}{r_s}\right)^n \frac{P_n^1(cos\theta_s)}{\sqrt{(1+\mathcal{R})^2 + \mathcal{R}^2}} \right]^2 \tag{4.7}$$

The expression for the power loss when using the perfect conductor model is obtained from (4.4), where H_θ at the conductor surface is calculated from (2.21) with A as given in (2.27)

and can be expressed in the form

$$P = \frac{\pi R_s}{2} \sum_{n=1}^{\infty} \frac{2n+1}{n(n+1)} \left[\sum_{s=1}^{N_t} I_s sin\theta_s \left(\frac{r_0}{r_s} \right)^n P_n^1(cos\theta_s) \right]^2 \tag{4.8}$$

Exact analytical solution for the power loss

The expression for the power loss from the exact analytical field solution for a conducting sphere can be obtained by integrating the Poynting vector ($\boldsymbol{S} = \frac{1}{2}\boldsymbol{E}_\varphi \times \boldsymbol{H}_\theta^*$) over the conductor surface and considering only the real part.

$$P = \frac{1}{2}\mathrm{Re} \oint_s (\boldsymbol{E}_\varphi \times \boldsymbol{H}_\theta^*)_{r=r_0} \cdot d\boldsymbol{s} \tag{4.9}$$

Equation (4.9) can be further simplified into the form

$$P = \pi r_0^2 \mathrm{Re} \int_0^\pi (E_\varphi H_\theta^*)_{r=r_0} sin\theta d\theta \tag{4.10}$$

E_φ and H_θ at the conductor surface are determined from (2.20) and (2.21), respectively, with the magnetic vector potential A as given in (F.13). For a system with a single inducing turn

$$\begin{aligned} E_\varphi\Big|_{r=r_0} &= \frac{-j\omega\mu_0}{2} I_s sin\theta_s \sum_{n=1}^{\infty} \frac{2n+1}{n(n+1)} \frac{r_0^{n-1}}{r_s^n} \frac{j_n(kr_0)}{j_{n-1}(kr_0)} P_n^1(cos\theta_s) P_n^1(cos\theta) \\ H_\theta\Big|_{r=r_0} &= \frac{-I_s sin\theta_s}{2} \sum_{n=1}^{\infty} \frac{r_0^{n-1}}{r_s^n} \left[\frac{1}{n} - \frac{\mathcal{X}_n}{n+1} \right] P_n^1(cos\theta_s) P_n^1(cos\theta) \end{aligned} \tag{4.11}$$

where $\mathcal{X}_n = \left[\frac{2n+1}{kr_0} \frac{j_n(kr_0)}{j_{n-1}(kr_0)} - 1 \right]$.

Substituting E_φ and H_θ in (4.10) and considering the orthogonality properties of the associated Legendre functions [see (C.10) in Appendix C], the exact analytical solution for the power loss can be expressed as

$$P = \frac{\pi\mu_0\omega I_s^2 sin^2\theta_s}{2}\mathrm{Re}\sum_{n=1}^{\infty}\frac{j}{k}\left(\frac{r_0}{r_s}\right)^{2n}\left[\frac{j_n(kr_0)}{j_{n-1}(kr_0)}\right]\left[\frac{1}{n}-\frac{\mathcal{X}_n}{n+1}\right]^*\left[P_n^1(cos\theta_s)\right]^2 \tag{4.12}$$

For a conducting sphere placed in an inducing system with N_t turns, the resultant power loss can be calculated from

$$P = \frac{\pi\mu_0\omega}{2}\mathrm{Re}\left\{\frac{j}{k}\sum_{n=1}^{\infty}r_0^{2n}\frac{j_n(kr_0)}{j_{n-1}(kr_0)}\left[\frac{1}{n}-\frac{\mathcal{X}_n}{n+1}\right]^*\left[\sum_{s=1}^{N_t}\frac{I_s sin\theta_s P_n^1(cos\theta_s)}{r_s^n}\right]^2\right\} \tag{4.13}$$

4.1.2 Losses in Conducting Spheroids

The losses due to the induced currents in the conducting spheroid can be computed approximately from (4.3), with the tangential component of the magnetic field intensity on the conductor surface obtained by using the impedance boundary conditions as discussed in Chapter-3,

$$P = \frac{1}{2}\oint_s R_s\left|H_\eta\right|^2_{\xi=\xi_0}\,ds \tag{4.14}$$

where the magnetic field intensity H_η at the conductor surface is determined from (3.33) for a prolate spheroid and from (3.48) for an oblate spheroid. The constants of integration C_n are determined as explained in Section-3.2.3 for both the SIBC and the impedance boundary condition with first order curvature correction. It is also seen that the real part of the surface impedance with first order curvature correction is the same as that of the standard surface impedance(see Appendix G). The surface integral in (4.14) is performed over the surface of the conducting spheroid, where the area element $ds = h_\eta h_\varphi d\eta d\varphi$, with h_η and h_φ being the scale factors in either prolate or oblate spheroidal coordinates [as given in (3.2) and (3.5)].

Perfect conductor model

The expression for the power loss when using this model can be obtained from (4.14), with H_η determined from (3.30) and A from (3.60) for a prolate spheroid. For an inducing system

with N_t number of turns, the resultant power loss due to induced currents is given in [1]

$$P = \frac{1}{2}\frac{\pi R_s I_0^2}{\sqrt{\xi_0^2-1}}\int_{-1}^{+1}\frac{1}{\sqrt{\xi_0^2-\eta^2}}\left[\sum_{s=1}^{N}\varepsilon_s[(1-\eta_s^2)(\xi_s^2-1)]^{1/2} \cdot \sum_{n=1}^{\infty}\frac{(2n+1)}{n(n+1)}\frac{P_n^1(\eta_s)Q_n^1(\xi_s)P_n^1(\eta)}{Q_n^1(\xi_0)}\right]^2 d\eta \tag{4.15}$$

for a prolate spheroid and

$$P = \frac{1}{2}\frac{\pi R_s I_0^2}{\sqrt{\xi_0^2+1}}\int_{-1}^{+1}\frac{1}{\sqrt{\xi_0^2+\eta^2}}\left[\sum_{s=1}^{N}\varepsilon_s[(1-\eta_s^2)(\xi_s^2+1)]^{1/2} \cdot \sum_{n=1}^{\infty}\frac{(2n+1)}{n(n+1)}\frac{P_n^1(\eta_s)Q_n^1(j\xi_s)P_n^1(\eta)}{Q_n^1(j\xi_0)}\right]^2 d\eta \tag{4.16}$$

for an oblate spheroid.

4.2 Forces Acting on Conducting Spheres and Spheroids

The force acting on induced solid conductors can be calculated by using the Maxwell stress tensor or by applying the principle of action and reaction, the force acting on the conducting body being equal in magnitude and opposite in direction to the force acting on the system of inducing turns. The latter method is employed in what follows. The force acting upon a filamentary current element due to an external magnetic field is given by

$$\Delta \boldsymbol{F} = I\Delta \boldsymbol{l} \times \boldsymbol{B}^{ext} \tag{4.17}$$

where $\Delta \boldsymbol{l}$ is the vector length element pointed in the direction of the current I carried by the filament and $\boldsymbol{B}^{ext}$ is the magnetic flux density at the conductor element due to all the sources except the current-carrying filamentary element upon which the force is calculated. Due to the axisymmetry of the system under study, the resulting force acting upon each turn is oriented in the z-direction. By considering the fact that the field quantities are in phasor

form, the resultant time-average force acting on the k-th turn can be expressed as [9]

$$\boldsymbol{F}_k = \frac{1}{2}\mathrm{Re}\left\{I_k^* \int_c (\boldsymbol{u}_\varphi \times \boldsymbol{B}_{\rho k}^{ext}) dl\right\} \tag{4.18}$$

where $B_{\rho k}^{ext}$ is the projection of the external magnetic flux density at the points on the k-th turn $\boldsymbol{B}_k^{ext}$ in a radial direction away from the z-axis, which is the only component contributing to the resultant force. The resultant time-average force acting on the sphere/spheroid is obtained by the superposition of the forces on individual turns. It should be noted that only the magnetic field produced by the induced currents contribute to the resultant force, since the resultant force acting on the system of inducing turns due only to the currents in these turns is equal to zero. This simplifies the computations, being sufficient to consider only the magnetic field produced by the induced currents $\boldsymbol{B}^{ind}$. Taking into account that $dl = b_k d\phi$, where b_k is the radius of the k-th inducing turn, (4.18) can be simplified as

$$F_k = \pi b_k \mathrm{Re}\left\{I_k^* B_{\rho k}^{ind}\right\} \tag{4.19}$$

4.2.1 Force Acting on a Conducting Sphere

Let's consider a conducting sphere in the presence of an inducing system with N_t turns. The total magnetic flux density due to the induced currents at the points on the k-th turn in a radial direction away from the z-axis can be determined from

$$B_{\rho k}^{ind} = B_{\theta k}^{ind} \boldsymbol{u}_\theta \cdot \boldsymbol{u}_\rho + B_{rk}^{ind} \boldsymbol{u}_r \cdot \boldsymbol{u}_\rho \tag{4.20}$$

Equation (4.20) can be further simplified by taking $\varphi = 0$, in the form

$$B_{\rho k}^{ind} = B_{\theta k}^{ind} cos\theta_k + B_{rk}^{ind} sin\theta_k \tag{4.21}$$

B_r^{ind} and B_θ^{ind} can be determined from the following expressions,

$$
\begin{aligned}
B_r^{ind} =& \frac{1}{r sin\theta} \frac{\partial}{\partial \theta} \left[sin\theta A^{ind} \right] \\
B_\theta^{ind} =& \frac{-1}{r} \frac{\partial}{\partial r} \left[r A^{ind} \right]
\end{aligned}
\tag{4.22}
$$

where A^{ind} is the magnetic vector potential produced by the induced currents and can be determined from (2.11), with C_n as given by (2.24). Thus,

$$
\begin{aligned}
B_{rk}^{ind} =& \frac{-\mu_0}{2} \sum_{s=1}^{N_t} I_s sin\theta_s \sum_{n=1}^{\infty} \left[\frac{(n+1) Z_s r_0^{2n+1} - j\omega\mu_0 r_0^{2(n+1)}}{n Z_s + j\omega\mu_0 r_0} \right] \frac{1}{r_s^n r_k^{n+2}} P_n^1(cos\theta_s) P_n(cos\theta_k) \\
B_{\theta k}^{ind} =& \frac{\mu_0}{2} \sum_{s=1}^{N_t} I_s sin\theta_s \sum_{n=1}^{\infty} \left[\frac{(n+1) Z_s r_0^{2n+1} - j\omega\mu_0 r_0^{2(n+1)}}{n Z_s + j\omega\mu_0 r_0} \right] \frac{1}{r_s^n r_k^{n+2}} \frac{P_n^1(cos\theta_s) P_n^1(cos\theta_k)}{n+1}
\end{aligned}
\tag{4.23}
$$

Substituting B_{rk}^{ind} and $B_{\theta k}^{ind}$ in (4.21), the resultant time-average force acting on the sphere can be expressed in the form.

$$
F = \frac{\pi\mu_0}{2} \sum_{k=1}^{N_t} I_k b_k \sum_{s=1}^{N_t} I_s sin\theta_s \sum_{n=1}^{\infty} \left[\frac{(n+1) Z_s r_0^{2n+1} - j\omega\mu_0 r_0^{2(n+1)}}{n Z_s + j\omega\mu_0 r_0} \right] \frac{1}{r_s^n r_k^{n+2}} \frac{P_n^1(cos\theta_s) \mathcal{K}_n(\theta_k)}{n+1}
\tag{4.24}
$$

where $\mathcal{K}_n(\theta_k) \equiv cos\theta_k P_n^1(cos\theta_k) - (n+1) sin\theta_k P_n(cos\theta_k)$. The expression for the force acting on a perfectly conducting sphere is obtained from (4.24) by assuming a zero surface impedance.

Exact analytical solution for the force

The magnetic vector potential due to the induced currents A^{ind}, when using the exact boundary conditions as given by (F.11) can be determined from (2.11), with C_n as given by (F.12). Thus from (4.22) we get

$$
\begin{aligned}
B_{rk}^{ind} =& \frac{-\mu_0}{2} \sum_{s=1}^{N_t} I_s sin\theta_s \sum_{n=1}^{\infty} \frac{r_0^{2n+1}}{r_s^n} r_k^{-(n+2)} \left[\frac{(2n+1)}{kr_0} \frac{j_n(kr_0)}{j_{n-1}(kr_0)} - 1 \right] P_n^1(cos\theta_s) P_n(cos\theta_k) \\
B_{\theta k}^{ind} =& \frac{\mu_0}{2} \sum_{s=1}^{N_t} I_s sin\theta_s \sum_{n=1}^{\infty} \frac{r_0^{2n+1}}{(n+1) r_s^n} r_k^{-(n+2)} \left[\frac{(2n+1)}{kr_0} \frac{j_n(kr_0)}{j_{n-1}(kr_0)} - 1 \right] P_n^1(cos\theta_s) P_n^1(cos\theta_k)
\end{aligned}
\tag{4.25}
$$

The exact analytical solution for the resultant time-average force acting on the sphere can be expressed in the form.

$$F = \frac{\pi\mu_0}{2}\sum_{k=1}^{N_t} I_k b_k \sum_{s=1}^{N_t} I_s sin\theta_s \sum_{n=1}^{\infty} \frac{r_0^{2n+1}}{r_s^n r_k^{n+2}} \left[\frac{2n+1}{kr_0}\frac{j_n(kr_0)}{j_{n-1}(kr_0)} - 1\right] \frac{P_n^1(cos\theta_s)\mathcal{K}_n'(\theta_k)}{(n+1)} \tag{4.26}$$

where $\mathcal{K}_n'(\theta_k) \equiv cos\theta_k P_n^1(cos\theta_k) - (n+1)sin\theta_k P_n(cos\theta_k)$.

4.2.2 Force Acting on Conducting Spheroids

The force acting on the conducting prolate/oblate spheroid can be determined from (4.19) where

$$B_{\rho k}^{ind} = B_{\eta k}^{ind}\boldsymbol{u}_\eta \cdot \boldsymbol{u}_\rho + B_{\xi k}^{ind}\boldsymbol{u}_\xi \cdot \boldsymbol{u}_\rho \tag{4.27}$$

The directions of the unit vectors, $\boldsymbol{u}_\eta, \boldsymbol{u}_\xi, \boldsymbol{u}_\varphi$, and $\boldsymbol{u}_\rho$ are as indicated in Fig.3.1 in prolate spheroidal coordinates and in Fig.3.2 in oblate spheroidal coordinates. The unit vectors $\mathbf{u}_\eta$ and $\mathbf{u}_\xi$ in (4.27) are given by

$$\begin{aligned} \mathbf{u}_\eta &= \frac{1}{h_\eta}\frac{\partial \boldsymbol{r}}{\partial \eta} \\ \mathbf{u}_\xi &= \frac{1}{h_\xi}\frac{\partial \boldsymbol{r}}{\partial \xi} \end{aligned} \tag{4.28}$$

and the position vector $\boldsymbol{r} = x\boldsymbol{u}_x + y\boldsymbol{u}_y + z\boldsymbol{u}_z$, in which x, y, z are expressed as in (3.1) and the scale factors h_η, h_ξ are as given in (3.2). Taking $\boldsymbol{u}_\rho$ at $\varphi = 0$ (i.e $\boldsymbol{u}_\rho = \boldsymbol{u}_x$) we have

$$\begin{aligned} \boldsymbol{u}_\eta \cdot \boldsymbol{u}_\rho &= \frac{-\eta(\xi^2-1)^{1/2}}{(\xi^2-\eta^2)^{1/2}} \\ \boldsymbol{u}_\xi \cdot \boldsymbol{u}_\rho &= \frac{\xi(1-\eta^2)^{1/2}}{(\xi^2-\eta^2)^{1/2}} \end{aligned} \tag{4.29}$$

$B_{\eta k}^{ind}$ and $B_{\xi k}^{ind}$ at the points on the k-th inducing turn can be determined from (3.30) and (3.31) with $A = A^{ind}$, which is the magnetic vector potential due to induced currents as

given in (3.19). The constants of integration C_n are determined as described in Section-3.2.3. For a conducting prolate spheroid in the presence of an inducing system with N_t turns, using the properties of the associated Legendre functions in (C.7) of Appendix C, we obtain

$$\begin{aligned} B_{\eta k}^{ind} =& \frac{1}{c\sqrt{\xi_k^2-\eta_k^2}} \sum_{s=1}^{N_t} I_s \sum_{n=1}^{\infty} C_n n(n+1) Q_n(\xi_k) P_n^1(\eta_k) \\ B_{\xi k}^{ind} =& \frac{-1}{c\sqrt{\xi_k^2-\eta_k^2}} \sum_{s=1}^{N_t} I_s \sum_{n=1}^{\infty} C_n n(n+1) P_n(\eta_k) Q_n^1(\xi_k) \end{aligned} \tag{4.30}$$

From (4.27), (4.29) and (4.30), the resultant flux density $B_{\rho k}^{ind}$ at k-th turn is derived in the form

$$\begin{aligned} B_{\rho k}^{ind} =& \frac{-1}{c\sqrt{\xi_k^2-\eta_k^2}} \sum_{s=1}^{N_t} I_s \sum_{n=1}^{\infty} C_n n(n+1) \left[\eta_k(\xi_k^2-1)^{1/2} Q_n(\xi_k) P_n^1(\eta_k) + \right. \\ & \left. \xi_k(1-\eta_k^2)^{1/2} P_n(\eta_k) Q_n^1(\xi_k)\right] \end{aligned} \tag{4.31}$$

The resultant force acting on the spheroid is obtained from (4.19) by taking into consideration the relationships given in (C.9) in Appendix C and by adding the forces acting on individual turns,

$$F = 2\pi \text{ Re } \sum_{k=1}^{N_t} I_k \frac{\left[(1-\eta_k^2)(\xi_k^2-1)\right]^{1/2}}{(\xi_k^2-\eta_k^2)} \sum_{s=1}^{N_t} I_s C_n n(n+1) \mathcal{K}_n(\eta_k, \xi_k) \tag{4.32}$$

where $\mathcal{K}_n(\eta_k, \xi_k) \equiv \frac{1}{n}\left[\eta_k Q_{n-1}^1(\xi_k) P_n^1(\eta_k) - \xi_k Q_n^1(\xi_k) P_{n-1}^1(\eta_k)\right]$.

In the case of a conducting oblate spheroid placed in an inducing system with N_t turns, the resultant force acting on the spheroid is derived from (4.32) with the transformation $(\xi \to j\xi, c \to -jc)$ in the form

$$F = 2\pi \text{ Re } \sum_{k=1}^{N_t} I_k \frac{\left[(1-\eta_k^2)(\xi_k^2+1)\right]^{1/2}}{(\xi_k^2+\eta_k^2)} \sum_{s=1}^{N_t} I_s C_n n(n+1) \mathcal{K}_n'(\eta_k, \xi_k) \tag{4.33}$$

where $\mathcal{K}_n'(\eta_k, \xi_k) \equiv \frac{1}{n}\left[j\eta_k Q_{n-1}^1(j\xi_k) P_n^1(\eta_k) + \xi_k Q_n^1(j\xi_k) P_{n-1}^1(\eta_k)\right]$.

Perfectly conducting spheroid

The force acting on a perfectly conducting spheroid can be determined from (4.19) with $B_{\eta k}^{ind}$ and $B_{\xi k}^{ind}$ obtained from (3.30) and (3.31), respectively, where the magnetic vector potential A^{ind} is as given in (3.19). The constants C_n are given in (3.59). The resultant time-average force acting on a prolate spheroid is given by [1]

$$\begin{aligned} F = & \frac{\pi\mu_0}{2} Real \sum_{k=1}^{N} I_k \frac{[(1-\eta_k^2)(\xi_k^2-1)]^{1/2}}{(\xi_k^2-\eta_k^2)} \sum_{s=1}^{N} I_s[(1-\eta_s^2)(\xi_s^2-1)]1/2 \\ & \cdot \sum_{n=1}^{\infty} \frac{P_n^1(\xi_0)}{Q_n^1(\xi_0)} P_n^1(\eta_s) Q_n^1(\xi_s) \mathcal{L}_n(\eta_k, \xi_k) \end{aligned} \tag{4.34}$$

where $\mathcal{L}_n(\eta_k, \xi_k) \equiv \frac{2n+1}{n^2(n+1)} \left[\xi_k P_{n-1}^1(\eta_k) Q_n^1(\xi_k) - \eta_k P_n^1(\eta_k) Q_{n-1}^1(\xi_k)\right]$. The expression for a perfectly conducting oblate spheroid is obtained from (4.34) by performing the transformation $\xi \rightarrow j\xi, c \rightarrow -jc$,

$$\begin{aligned} F = & \frac{\pi\mu_0}{2} Real \sum_{k=1}^{N} I_k \frac{[(1-\eta_k^2)(\xi_k^2+1)]^{1/2}}{(\xi_k^2+\eta_k^2)} \sum_{s=1}^{N} I_s[(1-\eta_s^2)(\xi_s^2+1)]1/2 \\ & \cdot \sum_{n=1}^{\infty} \frac{P_n^1(j\xi_0)}{Q_n^1(j\xi_0)} P_n^1(\eta_s) Q_n^1(j\xi_s) \mathcal{L}_n'(\eta_k, \xi_k) \end{aligned} \tag{4.35}$$

where $\mathcal{L}_n'(\eta_k, \xi_k) \equiv \frac{2n+1}{n^2(n+1)} \left[j\xi_k P_{n-1}^1(\eta_k) Q_n^1(j\xi_k) - \eta_k P_n^1(\eta_k) Q_{n-1}^1(j\xi_k)\right]$.

Chapter 5

Numerical Results and Conclusions

Numerical results have been computed for the power losses and the forces acting on conducting spheres and spheroids. In the case of a conducting sphere, the computed results generated by using both the PEC model and the SIBC are compared with the results obtained from the exact analytical solution. For conducting spheroids, the numerical results obtained with the PEC model and the SIBC are compared with experimental results presented in [1] and also with the the results obtained by using the impedance boundary condition with first order curvature correction. As an example, we consider an inducing system consisting of three equally spaced coaxial current-carrying turns in the presence of a conducting prolate spheroid as depicted in Fig. 5.1.

It is important to notice that the expressions derived for the power loss and the force acting on a conducting spheroid are functions of $2N_t+1$ (where N_t is the number of inducing turns) dimensionless geometric parameters, namely, ξ_0, η_s, ξ_s , $s = 1, 2...N_t$, of the semi-focal length c and of the currents I_s,$s = 1, 2...N_t$. By taking into account the relations (3.3) in the case of a prolate spheroid and (3.6) in the case of an oblate spheroid, one can determined the parameters ξ_0, η_s, ξ_s from the dimensionless parameters $b_0/a_0, b_0/b_1, \tan\beta, d_1/b_1$, and from the semi-major/semi-minor axis (see Fig.5.1). The ratio b_0/a_0 is such that $b_0/a_0 < 1$ for prolate spheroids and $b_0/a_0 > 1$ for oblate spheroids. The dimensions of the system shown in Fig. 5.1 and the dimensionless parameters are chosen such that, a comparison between the results obtained from the analytical solution and the experimental results presented in [1] is made possible. Numerical results are computed for inducing systems having a single

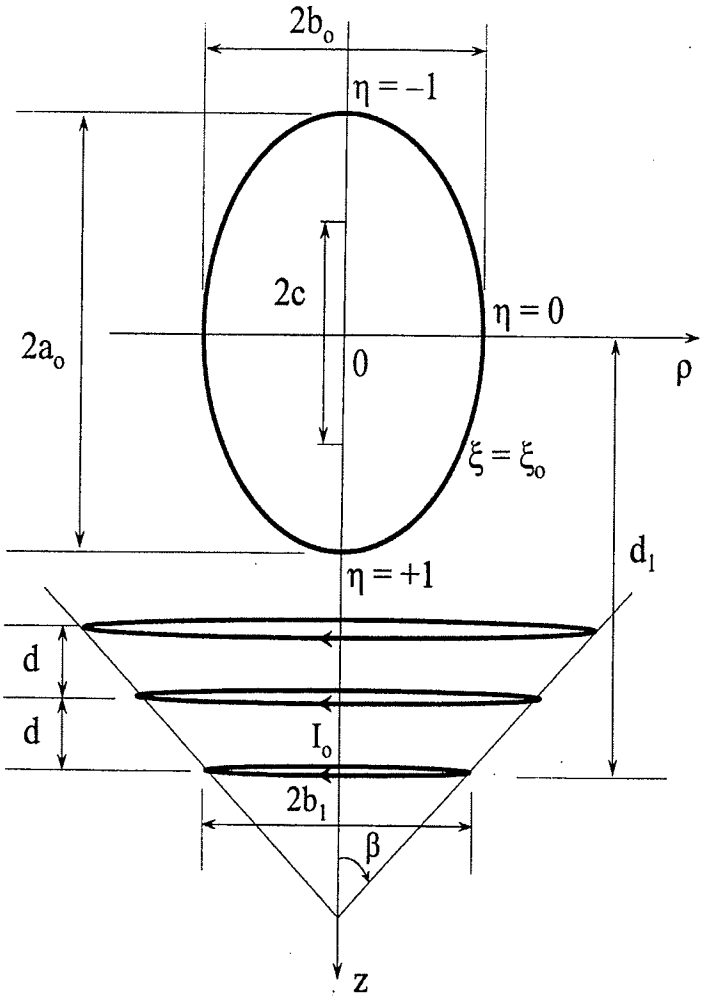

Figure 5.1: Conducting prolate spheroid in the presence of an inducing system with three coaxial current-carrying turns.

current-carrying turn and three current-carrying turns, which are displaced by a distance $d = b_1/4$.

In the case of a conducting sphere, the analytical solution for the power loss and for the force are functions of the geometric parameters r_0, r_s and θ_s, $s = 1, 2...N_t$, and of the currents I_s. The coordinates of the inducing turns (r_s and θ_s) are determined from the dimensionless parameters $r_o/b_1, \tan\beta$ and d_1/b_1, and from the radius r_0 of the sphere. In practical systems (e.g. electro-magnetic levitation systems) the inducing turns are connected in series, thus carrying the same current I_0. In the case of electromagnetic levitation systems,

stabilization turns are introduced in order to maintain the static stability [1], in which the direction of the currents is opposite to that of the currents in the main turns. Numerical results for the power losses normalized to $R_s I_0^2$ and the forces normalized to $\mu_0 I_0^2$ are calculated for various ratios of b_0/a_0 and d_1/b_1, and are plotted versus d_1/b_1. The same configuration of the inducing system as depicted in Fig. 5.1 is used with the induced conducting oblate spheroids and conducting spheres. The conductivity of the material (aluminum) is taken to be $\sigma = 3.77 \times 10^7 S/m$ and its permittivity and the permeability are assumed to be those of free space.

Numerical values for associated Legendre functions $P_n^1(z)$ and $Q_n^1(z)$ when $|z| < 1$ are calculated by using the recurrence formula as given in (C.13) in Appendix C. Numerical values for $Q_n^1(x)$ when $x > 1$ are calculated by using the algorithm in [16], while $Q_n^1(z)$ when $|z| > 1$ (in case of an oblate spheroid) are calculated from the subroutine in [17]. Numerical values for the modified Bessel functions of the first kind $I_{n+\frac{1}{2}}$ are calculated from the subroutine available in MATLAB.

5.1 Numerical Results for the Power Losses and for the Forces Acting on Conducting Spheres

The power losses and the forces acting on conducting spheres are evaluated numerically from the expressions derived in Chapter-4, by using

- the PEC model
- the SIBC model;
- the exact analytical solution.

Numerical results have been generated for inducing systems with a single current-carrying turn and also for systems with three current-carrying turns.

Table 5.1: Percentage truncation error of H_θ at the conductor surface for conducting spheres in the presence of a single inducing turn, with $r_0/b_1 = 1$ and $d_1/b_1 = 1$.

$\%\Delta\lvert H_\theta\rvert_{r=r_0}$							
		$\delta/r_0 = 1/5$			$\delta/r_0 = 1/20$		
θ^o	N	PEC	SIBC	Exact	PEC	SIBC	Exact
30	5	-210.31	-11.34	1.79	-210.31	-133.92	-133.02
	10	-126.53	-34.29	-49.31	-126.53	-89.01	-88.28
	15	15.59	27.94	5.89	15.59	93.29	9.35
	20	0.16	0.03	0.06	0.16	0.09	0.09
90	5	46.80	19.08	21.37	46.80	36.75	36.70
	10	-11.60	-3.61	-5.01	-11.60	-8.29	-8.23
	15	-0.03	0.03	-0.01	-0.03	-0.04	-0.01
	20	0.06	0.01	0.02	0.00	0.03	0.03
150	5	-13.37	-7.42	-8.86	-13.37	-11.06	-11.00
	10	-3.46	-1.54	-2.17	-3.46	-2.65	-2.63
	15	0.15	0.38	0.09	0.15	0.87	0.09
	20	0.13	0.03	0.08	0.13	0.08	0.08

Table 5.1 shows the effect of the number N of terms retained on the convergence of the infinite series in the expressions obtained for the tangential component of the magnetic field H_θ at the conductor surface at $\theta = 30°, 90°$ and $150°$ in the presence of a single inducing turn. The percentage error in the magnitude of H_θ when retaining a finite number of terms in the infinite series, is calculated with reference to the magnitude of H_θ calculated by retaining 25 terms. The computed results are presented for spheres having the ratio of the skin depth δ to the radius r_0, $\delta/r_0 = 1/5$ and $1/20$. The results obtained under the three different boundary conditions show that sufficiently accurate results (error less than 1%) can be obtained by considering only the first 20 terms.

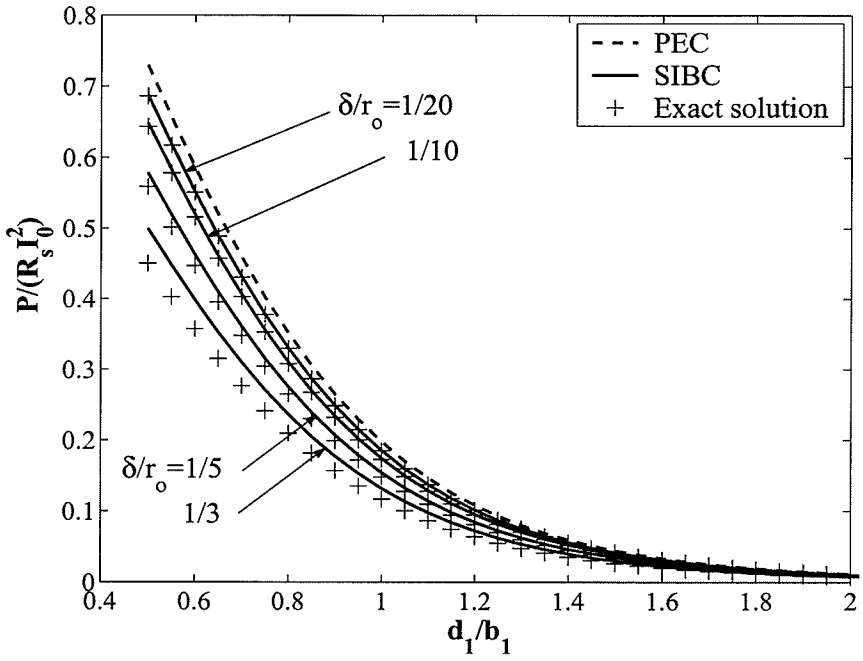

Figure 5.2: Normalized power losses in conducting spheres in the presence of a single inducing turn as a function of d_1/b_1, for different ratios of δ/r_0, with r_0/b_1=0.5.

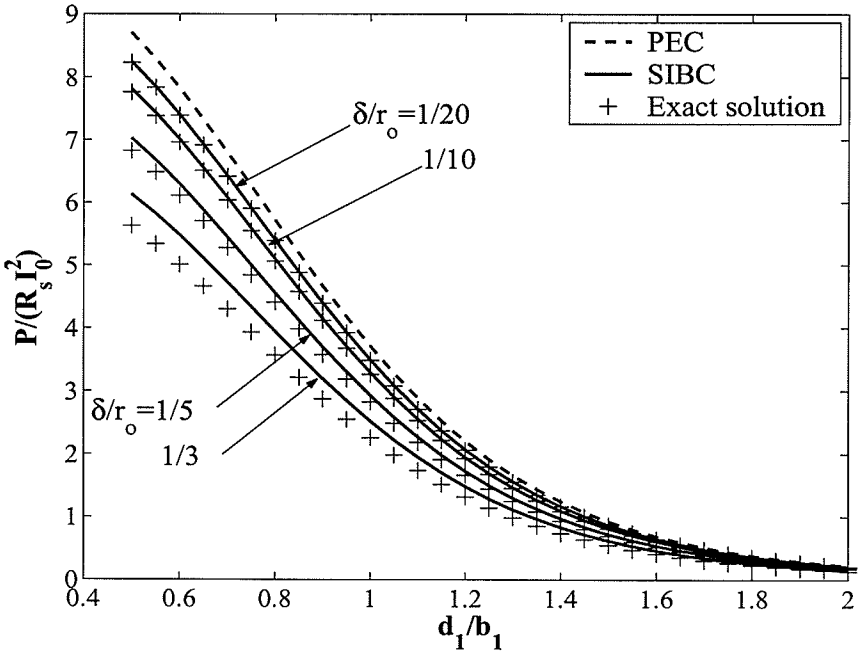

Figure 5.3: Normalized power losses in conducting spheres in the presence of three inducing turns as a function of d_1/b_1, for different ratios δ/r_0, with r_0/b_1=0.5, $d = b_1/4$, and $\tan\beta = 0$.

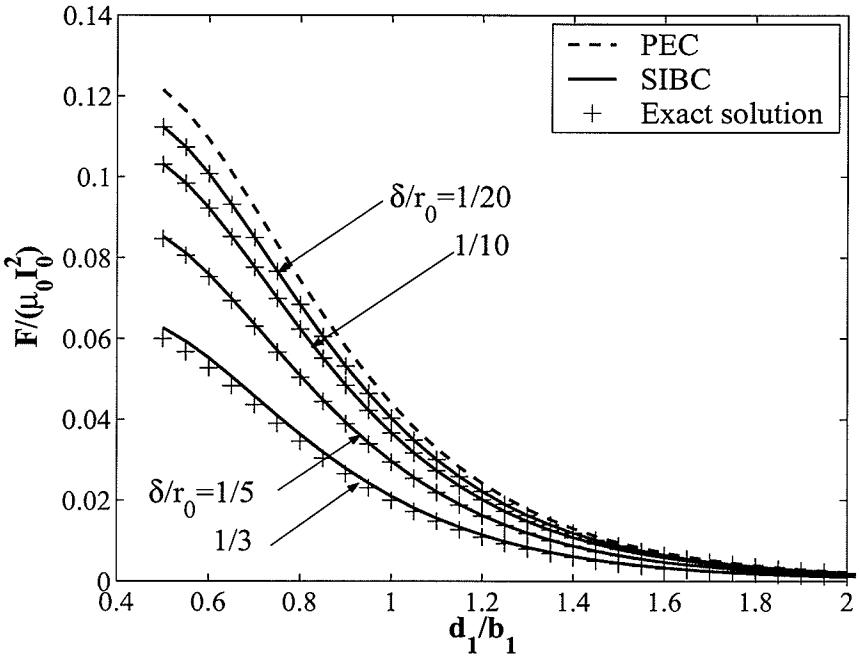

Figure 5.4: Normalized forces acting on conducting spheres in the presence of a single inducing turn as a function of d_1/b_1, for different ratios of δ/r_0, with r_0/b_1=0.5.

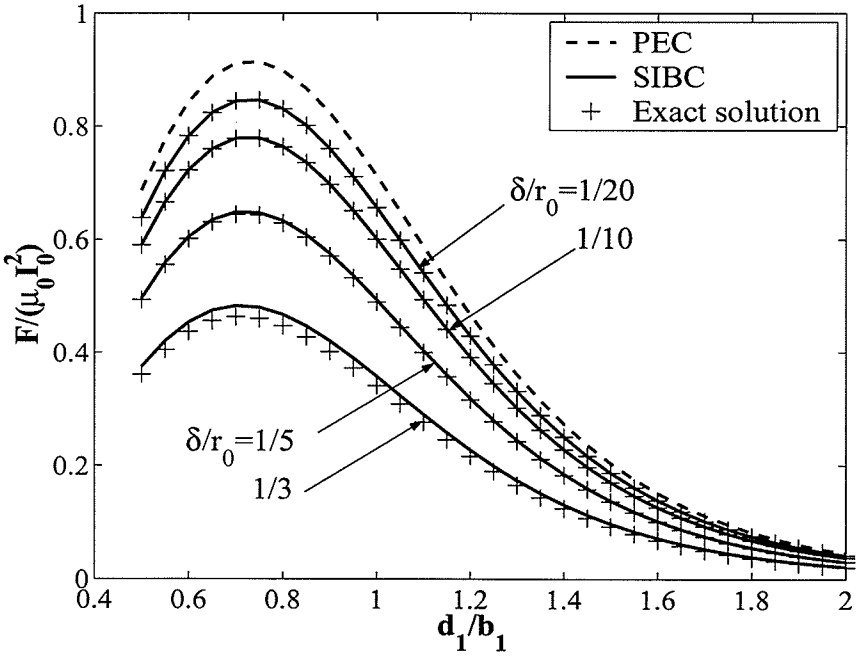

Figure 5.5: Normalized forces acting on conducting spheres in the presence of three inducing turns as a function of d_1/b_1, for different ratios δ/r_0, with r_0/b_1=0.5, $d = b_1/4$, and $\tan\beta = 0$.

Table 5.2: Maximum percentage error of the power loss and the force acting on spheres for different ratios of δ/r_0, where $r_0/b_1 = 0.5$.

Maximum Percentage Error								
	Single inducing turn				Three inducing turns			
	Power loss		Force		Power loss		Force	
δ/r_0	PEC	SIBC	PEC	SIBC	PEC	SIBC	PEC	SIBC
1/35	3.79	0.07	3.76	0.01	3.76	0.07	5.06	0.01
1/30	4.45	0.10	5.47	0.01	4.42	0.09	5.95	0.01
1/25	5.38	0.14	7.25	0.01	5.34	0.13	7.22	0.01
1/20	6.81	0.22	9.23	0.02	6.76	0.22	9.19	0.02
1/15	9.27	0.39	12.69	0.04	9.20	0.38	12.65	0.04
1/10	14.51	0.99	20.31	0.13	14.40	0.89	20.23	0.13
1/5	33.42	4.04	50.49	1.02	33.14	3.98	50.25	1.00
1/3	69.41	13.12	122.80	5.21	68.74	12.94	122.10	5.19

Figures 5.2 and 5.3 show the computed results for the power loss normalized to $R_s I_0^2$ versus the ratio d_1/b_1, for different ratios the skin depth to the radius of the sphere δ_0/r_0, for inducing systems having single and three current-carrying turn/s, respectively. Figures 5.4 and 5.5 show the computed results for the force normalized to $\mu_0 I_0^2$ versus the ratio d_1/b_1 for different ratios δ_0/r_0, for inducing systems having single and three current-carrying turn/s, respectively. Numerical results obtained for the power losses and the forces by using both the PEC model and the SIBC, are compared with the results obtained by solving the exact analytical solution. The maximum percentage errors in the results obtained for the range $d_1/b_1 \in (0.5, 2)$ with both the PEC model and the SIBC are determined by comparing them with the numerical results obtained from the exact analytical solution, and are tabulated in Table. 5.2. These results show that the maximum percentage error with the SIBC is less than 1% for skin depths of less than one tenth of the radius of the sphere, whereas the maximum percentage error for skin depths about one fifth of the radius is still less than 5%. It should be remarked that the normalized power loss and the normalized force obtained

from both the SIBC and the exact analytical solution are depend only on the ratio δ/r_0, being the same for the same ratios, r_0/b_1 and d_1/b_1 for a given configuration of the inducing system. The normalized power loss and the normalized force obtained by using the PEC model are independent of the frequency of the inducing field and the sphere material, being the same for systems which are geometrically similar.

5.2 Numerical Results for the Power Losses and for the Forces Acting on Conducting Spheroids

The numerical results for the power losses and the forces acting on conducting spheroids are obtained for different impedance boundary conditions, as discussed in Chapter 4, by using

- the PEC model;
- the SIBC model;
- the impedance boundary condition with first order curvature correction.

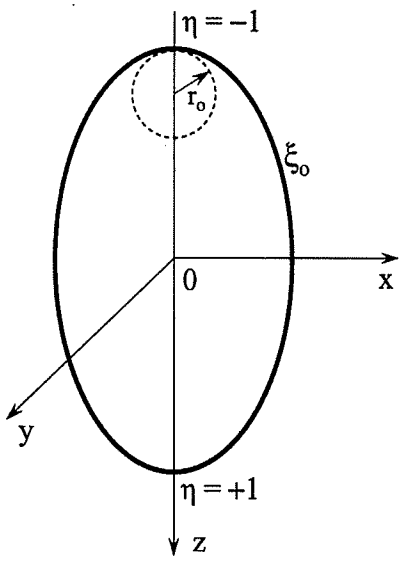

Figure 5.6: Radius of principal curvature at $\eta = -1$ for a prolate spheroid.

Table 5.3 shows the percentage error due to the truncation of the infinite series in the expressions derived for the tangential magnetic field intensity H_η at the conductor surface by using the approximate boundary conditions mentioned above. The parameters of the conducting spheroids are chosen such that $b_0/a_0 = 0.6$, $b_0/b_1 = 0.75$, $d_1/b_1 = 1.25$, $a_0 = 25$mm

for the prolate spheroid and $b_0/a_0 = 1.25$, $b_0/b_1 = 1$, $d_1/b_1 = 0.8$, $a_0 = 12$mm for the oblate spheroid. For the prolate spheroid the smallest radius of curvature (i.e. r_0 in Fig.5.6) calculated from either (E.4) or (E.7), at $\eta = \pm 1$ is approximately ten times the skin depth, namely $r_0 = 9$mm and $\delta = 0.916$mm at 8kHz. For the oblate spheroid the smallest radius of curvature at $\eta = 0$ is calculated from (E.9), namely, $r_0 = 9$mm is also approximately ten times the skin depth at 8kHz.

Table 5.3: Percentage truncation error of H_η at the conducting spheroid surfaces in the presence of a single inducing turn with, $b_0/a_0 = 0.6$, $b_0/b_1 = 0.75$, $d_1/b_1 = 1.25$, $a_0 = 25$mm for the prolate spheroid and $b_0/a_0 = 1.25$, $b_0/b_1 = 1$, $d_1/b_1 = 0.8$, $a_0 = 12$mm for the oblate spheroid.

$\%\triangle\lvert H_\eta\rvert_{\xi=\xi_0}$							
		Prolate spheroid			Oblate spheroid		
η	N	PEC	SIBC	CIBC[1]	PEC	SIBC	CIBC[1]
-0.95	10	22.564	15.618	15.648	47.900	29.245	29.495
	15	-5.654	-3.535	-3.557	8.053	4.497	4.568
	20	0.013	0.026	0.027	2.571	1.185	1.203
	25	-0.036	-0.025	-0.025	-1.084	-0.440	-0.442
0	10	-3.096	-2.465	-2.459	-8.521	-5.361	-5.385
	15	-0.033	-0.008	-0.032	1.005	0.538	0.542
	20	0.006	0.001	-0.021	-0.289	-0.136	-0.137
+0.95	10	0.965	0.732	0.735	3.245	2.176	2.168
	15	-0.027	-0.035	-0.035	-2.324	-1.315	-1.317
	20	-0.003	-0.002	-0.001	0.144	0.068	0.069

The numerical results tabulated in Table. 5.3 show that sufficiently accurate results(less than 1% error) can be obtained by only considering the first 20 terms in the infinite series in (3.33) in case of a prolate spheroid and only considering the first 25 terms in (3.48) for an oblate spheroid. Numerical values for the constants of integration C_n are determined as explained in Section 3.2.3, where integrals (3.44) and (3.54) are evaluated numerically by using the adaptive Gauss-Lobatto quadrature (available in MATLAB) with the absolute error tolerance specified at 10^{-6}.

[1]Corrected impedance boundary condition

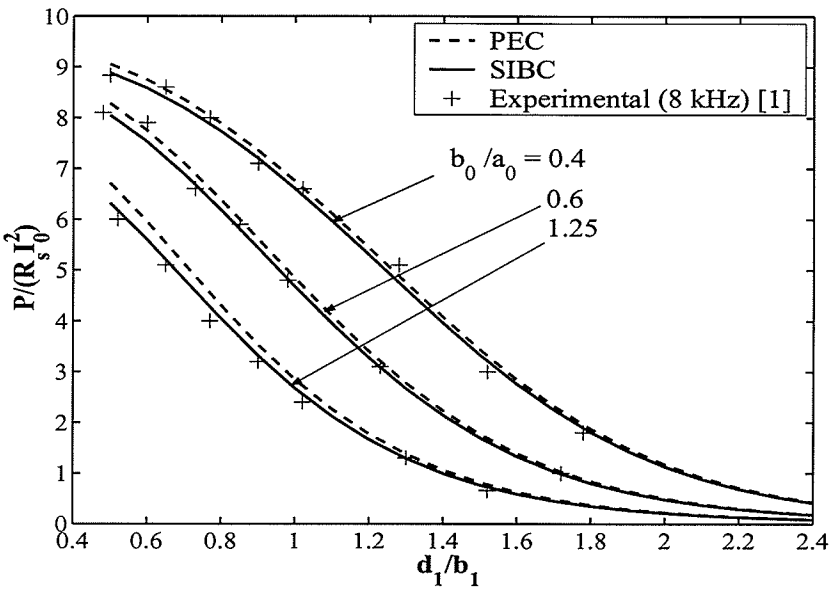

Figure 5.7: Normalized power losses in conducting spheroids as a function of d_1/b_1 for $\delta/b_0 = 0.0458$, with b_0/b_1=0.5, $d = b_1/4$ and tanβ =0.4.

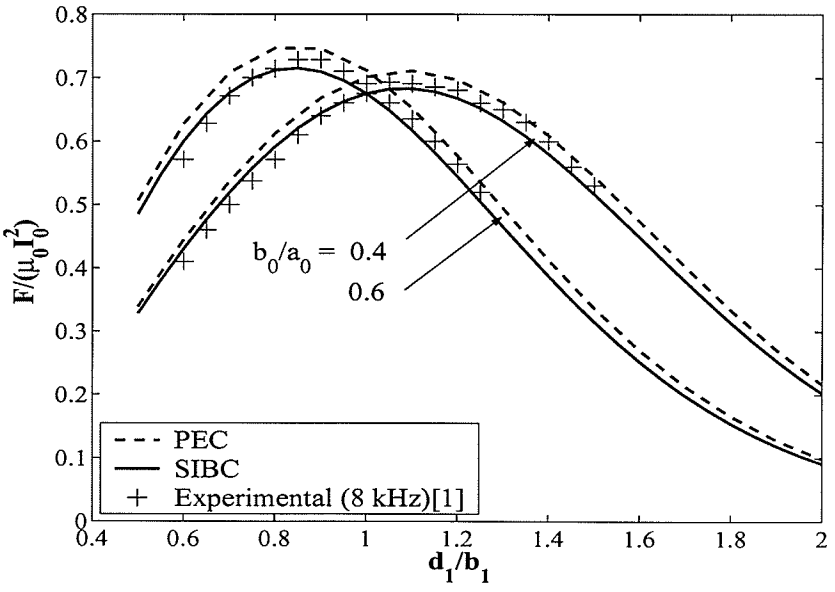

Figure 5.8: Normalized forces acting on conducting spheroids as a function of d_1/b_1 for $\delta/b_0 = 0.0458$, with b_0/b_1=0.5, $d = b_1/4$, and tanβ=0.4.

Figure 5.7 shows the power loss normalized to $R_s I_0^2$ in conducting spheroids as a function of the ratio d_1/b_1, obtained by using both the PEC and the SIBC, plotted along with the experimental results presented in [1]. Figure 5.8 shows the force normalized to $\mu_0 I_0^2$ as a function of d_1/b_1 for both the PEC and the SIBC, together with the experimental results presented in [1]. In Fig. 5.9, numerical results obtained for the normalized force acting on a conducting prolate spheroid with $b_0/a_0 = 0.6$ in the presence of three current-carrying turns at two different frequencies, 4kHz(at which $\delta = 1.296$mm) and 2kHz($\delta = 1.833$mm) are plotted together with experimental results presented in [1].

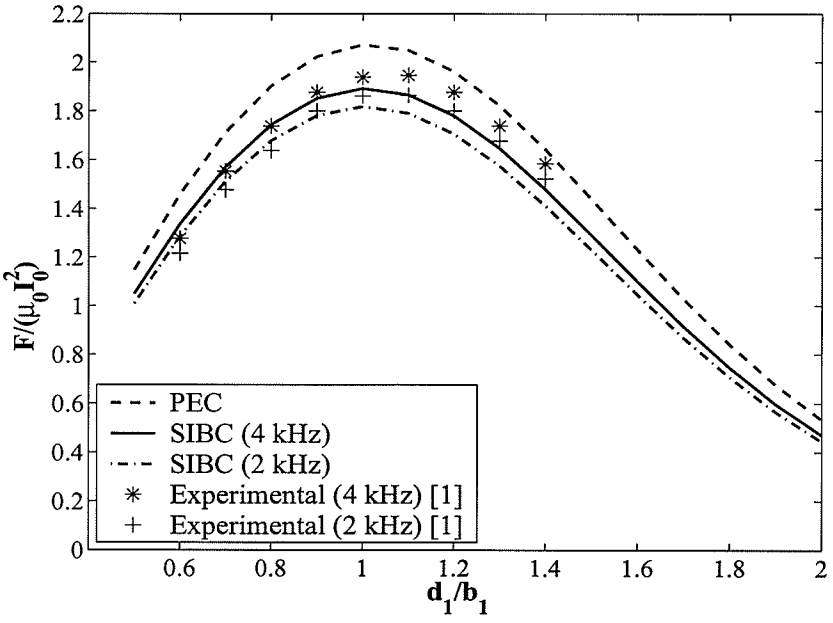

Figure 5.9: Normalized forces acting on conducting spheroids at two different frequencies as a function of d_1/b_1 , with $d = b_1/4$, $\tan\beta$=0.4, b_0/b_1=0.75, b_0/a_0=0.6 and $b_0 = 20$mm.

Figures 5.10 and 5.11 show the numerical results obtained for the normalized power loss and the normalized force for conducting spheroids having different axial ratios in the presence of a single inducing turn. Figures 5.12 and 5.13 show the normalized power loss and the normalized force acting on conducting spheroids having different axial ratios in the presence of three circular current-carrying turns.

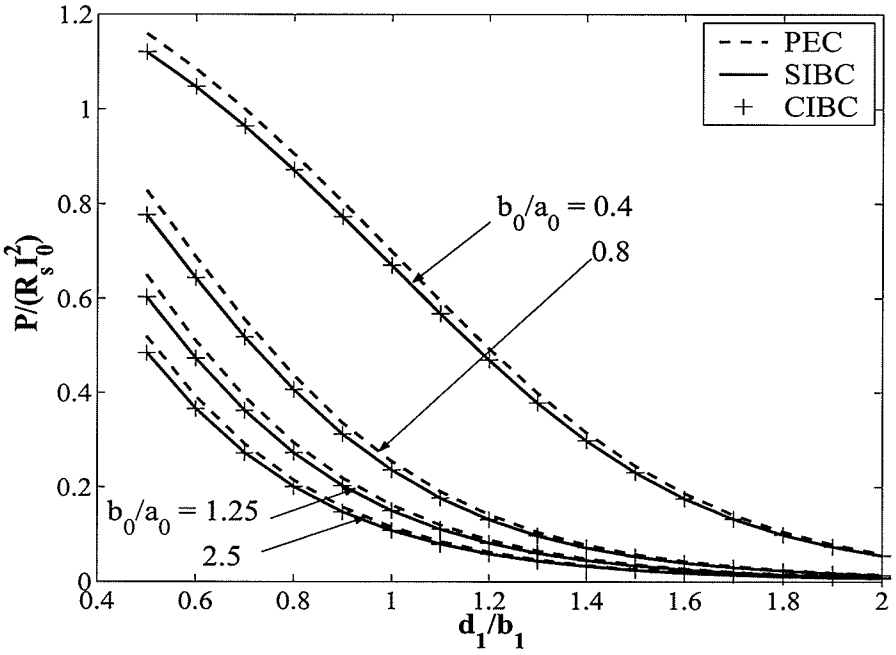

Figure 5.10: Normalized power losses in conducting spheroids in the presence of a single inducing turn as a function of d_1/b_1, for different ratios b_0/a_0, with b_0/b_1=0.5 and $\delta/b_0 = 1/15$ for prolate spheroids and $\delta/a_0 = 1/15$ for oblate spheroids.

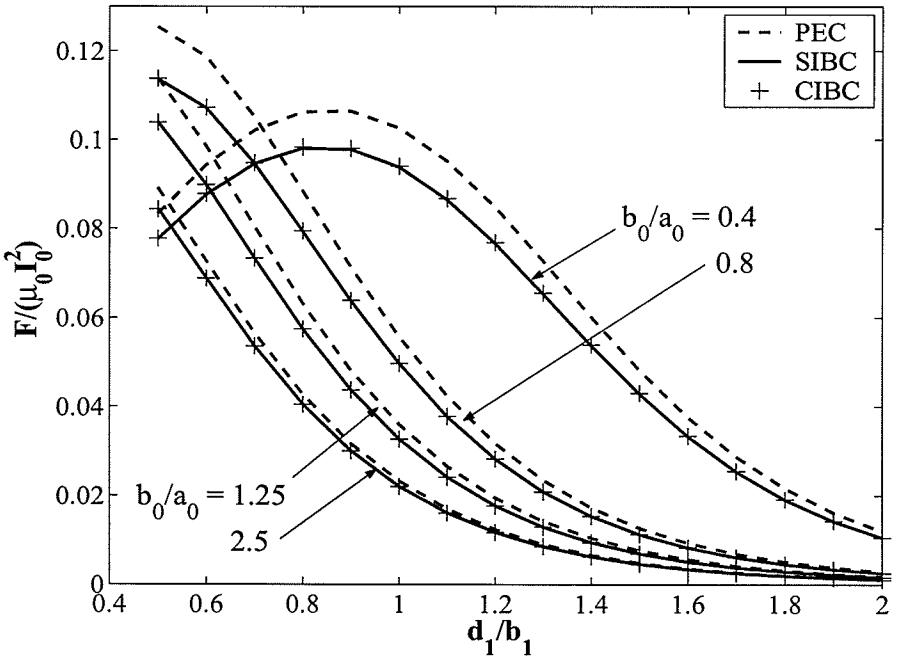

Figure 5.11: Normalized force acting on conducting spheroids in the presence of a single inducing turn as a function of d_1/b_1, for different ratios b_0/a_0, with b_0/b_1=0.5 and $\delta/b_0 = 1/15$ for prolate spheroids and $\delta/a_0 = 1/15$ for oblate spheroids.

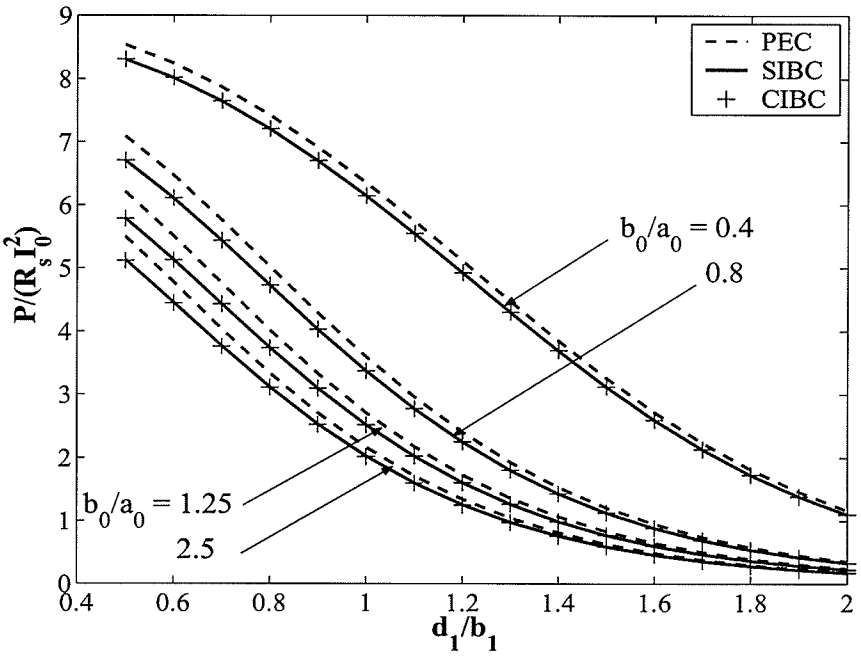

Figure 5.12: Normalized power losses in conducting spheroids in the presence three inducing turns as a function of d_1/b_1, for different ratios b_0/a_0, with b_0/b_1=0.5, $d = b_1/4$, $\beta = 30°$, and $\delta/b_0 = 1/15$ for prolate spheroids and $\delta/a_0 = 1/15$ for oblate spheroids,.

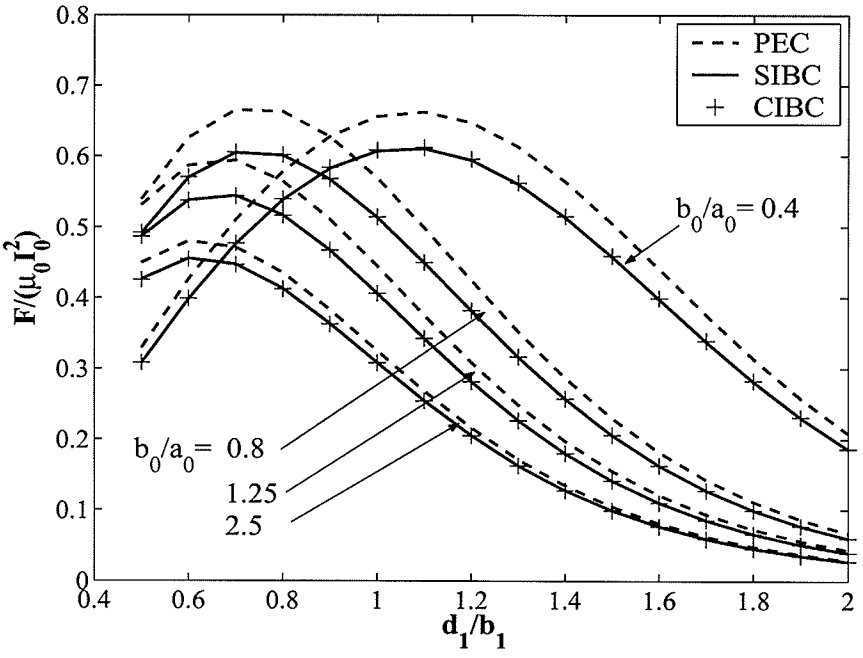

Figure 5.13: Normalized force acting on conducting spheroids in the presence of three inducing turns as a function of d_1/b_1, for different ratios b_0/a_0, with b_0/b_1=0.5, $d = b_1/4$, $\beta = 30°$, and $\delta/b_0 = 1/15$ for prolate spheroids and $\delta/a_0 = 1/15$ for oblate spheroids.

It has also been noticed that in the case of a conducting sphere, the surface impedance with first order curvature correction is the same as the standard surface impedance derived on the basis of the exact solution for a semi-space of good conductor. Thus, the computed results for the normalized power losses and for the normalized forces on conducting spheres, by using both the SIBC and the CIBC have the same accuracy with respect to the results obtained from the exact analytical solution. From the results obtained in Section 5.1 for a conducting sphere, it is seen that the maximum percentage error in the SIBC(which is same as that of the CIBC) with respect to the exact analytical solution is below 5% for skin depths less than one fifth of the radius. Based on this observation, it is reasonable to assume that the percentage error in the CIBC with respect to the exact analytical solution, in the case of a conducting spheroid having the smallest radius of normal curvature at least five times the skin depth is much less than 5%, when compared to that of a conducting sphere with the radius five times the skin depth.

In the absence of exact analytical results for conducting spheroids we can use as reference the results obtained from the curvature corrected impedance boundary condition(CIBC) in order to compare the performance of both the SIBC and the PEC model. It should be stressed that this argument is more applicable for the spheroids having the smallest radius of normal curvature at least five times the skin depth. Tables 5.4 and 5.5 show the maximum percentage error in the computed results for the normalized power losses obtained by using both the PEC model and the SIBC with respect to the CIBC, for conducting spheroids having different axial ratios($b_0/a_0 = 0.4, 0.8, 1.25$ and 2.5), in the presence of a single inducing turn in the range $d_1/b_1 \in$ (0.5,2). The dimensions of the spheroids are chosen such that the semi-minor axis (i.e. b_0 in case of a prolate spheroid and a_0 for an oblate spheroid) is an integer multiple of the skin depth δ. Tables 5.6 and 5.7 present the maximum percentage error in normalized forces obtained from PEC model and the SIBC with respect to the CIBC, for spheroids having different axial ratios in the presence of a single inducing turn in the range $d_1/b_1 \in$ (0.5,2).

Table 5.4: Maximum percentage error for the power loss in conducting prolate spheroids obtained from the PEC model and the SIBC with respect to the CIBC in the presence of a single inducing turn for various ratios δ/b_0 and $d_1/b_1 \in (0.5,2)$.

Maximum Percentage Error in Power Loss					
	$b_0/a_0 = 0.4$			$b_0/a_0 = 0.8$	
δ/b_0	PEC	SIBC	δ/b_0	PEC	SIBC
1/10	9.338	0.369	1/10	11.942	0.140
1/15	6.288	0.170	1/15	7.893	0.064
1/20	4.390	0.097	1/20	5.893	0.036
1/25	3.802	0.063	1/25	4.701	0.023
1/30	3.175	0.043	1/30	3.910	0.016
1/35	2.725	0.032	1/35	3.347	0.012

Table 5.5: Maximum percentage error for the power loss in conducting oblate spheroids obtained from the PEC model and the SIBC with respect to the CIBC in the presence of a single inducing turn for various ratios δ/b_0 and $d_1/b_1 \in (0.5,2)$.

Maximum Percentage Error in Power Loss					
	$b_0/a_0 = 1.25$			$b_0/a_0 = 2.5$	
δ/a_0	PEC	SIBC	δ/a_0	PEC	SIBC
1/10	12.182	0.073	1/10	11.340	0.569
1/15	7.995	0.034	1/15	7.360	0.270
1/20	5.949	0.020	1/20	5.441	0.157
1/25	4.736	0.013	1/25	4.315	0.103
1/30	3.934	0.009	1/30	3.574	0.072
1/35	3.364	0.007	1/35	3.050	0.054

Table 5.6: Maximum percentage error for the force acting on conducting prolate spheroids obtained from the PEC model and the SIBC with respect to CIBC in the presence of a single inducing turn for various ratios δ/b_0 and $d_1/b_1 \in (0.5,2)$.

Maximum Percentage Error in Force					
	$b_0/a_0 = 0.4$			$b_0/a_0 = 0.8$	
δ/b_0	PEC	SIBC	δ/b_0	PEC	SIBC
1/10	20.712	0.883	1/10	19.771	0.270
1/15	13.161	0.380	1/15	12.473	0.118
1/20	9.641	0.210	1/20	9.106	0.066
1/25	7.606	0.133	1/25	7.170	0.042
1/30	6.280	0.092	1/30	5.911	0.029
1/35	5.348	0.067	1/35	5.029	0.021
1/40	4.656	0.051	1/40	4.376	0.016

Table 5.7: Maximum percentage error for the force acting on conducting oblate spheroids obtained from the PEC model and the SIBC with respect to CIBC in the presence of a single inducing turn for various ratios δ/b_0 and $d_1/b_1 \in (0.5,2)$.

Maximum Percentage Error in Force					
	$b_0/a_0 = 1.25$			$b_0/a_0 = 2.5$	
δ/a_0	PEC	SIBC	δ/a_0	PEC	SIBC
1/10	15.819	0.191	1/10	8.918	0.402
1/15	10.057	0.086	1/15	5.715	0.184
1/20	7.369	0.048	1/20	4.200	0.105
1/25	5.813	0.031	1/25	3.318	0.068
1/30	4.800	0.022	1/30	2.742	0.047
1/35	4.087	0.016	1/35	2.336	0.035

Numerical results presented in above tables show that the results obtained by using the SIBC are in good agreement with the results obtained from the CIBC, with the maximum percentage difference between them in the range $d_1/b_1 \in (0.5, 2)$ and $\delta/b_0 \leq 1/10$ for prolate spheroids and $\delta/a_0 \leq 1/10$ for oblate spheroids is less than 1%. It is also remarked that the numerical results obtained for the normalized power loss and the normalized force for conducting spheroids depend only on the ratio δ/b_0(for prolate spheroids) or δ/a_0(for oblate spheroids), being the same for the same ratios, $b_0/a_0, b_0/b_1, d_1/b_1$ and for a given configuration of the inducing system.

5.3 Conclusions

In this thesis, the performance of various impedance boundary conditions for axisymmetric eddy-current problems is investigated. The perfect electric conductor boundary condition, the standard impedance boundary condition and the impedance boundary condition with first order curvature correction are used to solve analytically the Laplace equation for the magnetic vector potential in both spherical and spheroidal coordinates. The numerical results obtained for the normalized power losses and the normalized forces by using the SIBC are in good agreement with the experimental results presented in [1] (see Fig. 5.7, 5.8 and 5.9). The numerical results generated for conducting spheres using the above mentioned boundary conditions are compared with numerical results obtained from the exact analytical solution. The results in Table 5.2 show that the maximum percentage error in the SIBC is less than 1% for skin depths less than one tenth of the radius of the sphere, whereas numerical results with error below 5% can be achieved for skin depths about one fifth of the radius. In the case of conducting spheroids it is observed that the error in the results obtained for the normalized power losses and the normalized forces by using the SIBC with respect to the CIBC is below 1% for skin depths less than 1/10 of the semi-minor axis (see Tables 5.4, 5.5, 5.6, and 5.7).

On the other hand, one can apply the simpler PEC model at higher frequencies where the skin depth is significantly smaller than the dimensions of the conducting object. In the case

of a conducting sphere, from the results tabulated in Table 5.2, it can be concluded that sufficiently accurate results (error less than 5%) can be obtained for skin depths less than 1/35, of the radius of the sphere. Similar observation can be made from Tables 5.4, 5.5, 5.6 and 5.7 for conducting spheroids, where the maximum percentage error in the results obtained by using PEC model with respect to CIBC is less than 5% for normalized power losses for both prolate and oblate spheroids, when skin depth is less than 1/35 of the semi-minor axis. From the computed results obtained for the normalized force acting on conducting spheroids it is observed that in order to obtain an error below 5%, the semi-minor axis should be at least 35 times for oblate spheroids and 40 times for prolate spheroids than the skin depth .

5.4 Future Work

In this thesis the performance of the standard impedance boundary condition, the curvature corrected impedance boundary condition and the perfect electric conductor model for axisymmetric eddy-current problems has been studied. This work can be extended to study the performance of higher order impedance boundary conditions for the analysis of the quasistationary magnetic fields. Moreover the derivation of the exact analytical solution for a conducting spheroid will be highly useful when determining the accuracy of various approximate boundary conditions, since spheroids can be used to approximate different geometrical shapes those appear in many engineering applications.

Appendix A

Surface Impedance and Skin Depth of a Linear, Isotropic, Homogeneous, Lossy Conducting Semi-Space

Let us consider a time-harmonic uniform plane wave at normal incidence upon a lossy conducting medium of conductivity σ, as shown in Fig. A.1.

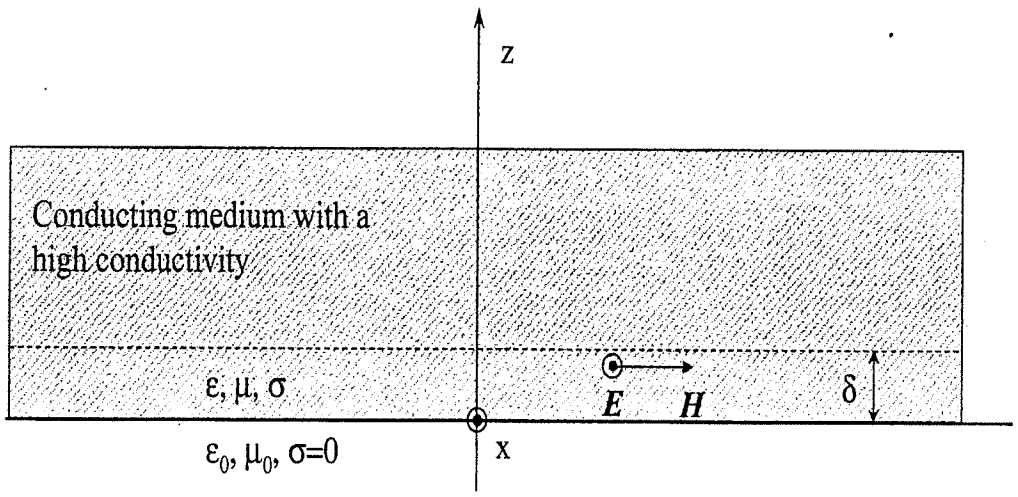

Figure A.1: Uniform plane wave travelling normal to a lossy conducting medium.

Inside the conducting material, the field quantities $\boldsymbol{E}$, $\boldsymbol{H}$ satisfy the Maxwell equations

$$\nabla \times \boldsymbol{H} = (\sigma + j\omega\epsilon)\boldsymbol{E} \tag{A.1}$$

$$\nabla \times \boldsymbol{E} = -j\omega\mu\boldsymbol{H} \tag{A.2}$$

$$\nabla \cdot \boldsymbol{E} = 0 \tag{A.3}$$

$$\nabla \cdot \boldsymbol{H} = 0 \tag{A.4}$$

From (A.1) amd (A.2)

$$\nabla^2 \boldsymbol{E} - \gamma^2 \boldsymbol{E} = 0 \tag{A.5}$$

$$\nabla^2 \boldsymbol{H} - \gamma^2 \boldsymbol{H} = 0 \tag{A.6}$$

The propagation constant $\gamma = [j\omega\mu(\sigma + j\omega\epsilon)]^{1/2} = \alpha + j\beta$, where α and β are the attenuation constant and the phase constant, respectively,

$$\alpha = \omega\sqrt{\mu\epsilon}\left\{\frac{1}{2}\left[\sqrt{\left(\frac{\sigma}{\omega\epsilon}\right)^2 + 1} - 1\right]\right\}^{1/2} \tag{A.7}$$

$$\beta = \omega\sqrt{\mu\epsilon}\left\{\frac{1}{2}\left[\sqrt{\left(\frac{\sigma}{\omega\epsilon}\right)^2 + 1} + 1\right]\right\}^{1/2} \tag{A.8}$$

In rectangular coordinates (A.5) and (A.6) can be reduced to scalar wave equations

$$\nabla^2 E_x - \gamma^2 E_x = 0 \tag{A.9}$$

$$\nabla^2 H_y - \gamma^2 H_y = 0 \tag{A.10}$$

with E_x and H_y depending only on z, the solutions for E_x and H_y giving waves propagating

in the positive z-direction can be expressed as

$$E_x(z) = E_0 e^{-\gamma z} \tag{A.11}$$

$$H_y(z) = H_0 e^{-\gamma z} \tag{A.12}$$

By substituting (A.11) and (A.12) in (A.2), H_0 can be expressed as $H_0 = \gamma E_0 / j\omega\mu$. The surface impedance Z_s is defined in terms of the tangential components of $\boldsymbol{E}$ and $\boldsymbol{H}$ such that $Z_s = E_{tan}/H_{tan}$ at the conductor surface,

$$Z_s = \frac{j\omega\mu}{\gamma} = \sqrt{\frac{j\omega\mu}{\sigma + j\omega\epsilon}} \tag{A.13}$$

The skin depth (δ) is defined as the distance from the surface at which the waves propagating in the lossy medium reduce in magnitude to $e^{-1} \cong 0.368$ from the value at the surface. In the case of a good conductor the term $(\sigma/\omega\epsilon)^2 \gg 1$, thus

$$\alpha = \beta = \sqrt{\frac{\omega\mu\sigma}{2}} \tag{A.14}$$

Similarly from (A.13) for a good conductor Z_s can be approximated by

$$Z_s = \sqrt{\frac{\omega\mu}{2\sigma}}(1+j) = R_s(1+j) \tag{A.15}$$

where $R_s = \sqrt{\omega\mu/2\sigma}$ is called the surface resistance. The skin depth δ for a good conductor can be approximated by

$$\delta = \frac{1}{\alpha} \cong \sqrt{\frac{2}{\omega\mu\sigma}} \tag{A.16}$$

Appendix B

Derivation of the Vector Potential Equations

Let's consider the vector relation

$$\nabla \times \nabla \times \boldsymbol{A} = \nabla(\nabla \cdot \boldsymbol{A}) - \nabla^2 \boldsymbol{A} \tag{B.1}$$

Suppose $\boldsymbol{A}$ satisfies the Coulomb gauge $\nabla \cdot \boldsymbol{A} = 0$. Thus

$$\nabla^2 \boldsymbol{A} = -\nabla \times \nabla \times \boldsymbol{A} \tag{B.2}$$

Let v_1, v_2 and v_3 be a system of orthogonal curvilinear coordinates with the scale factors h_1, h_2 *and* h_3, respectively. In this coordinate system $\boldsymbol{A} = A_1\boldsymbol{u}_1 + A_2\boldsymbol{u}_2 + A_3\boldsymbol{u}_3$ and the curl($\boldsymbol{A}$) is given by

$$\nabla \times \boldsymbol{A} = \frac{1}{h_1 h_2 h_3} \begin{vmatrix} h_1\boldsymbol{u}_1 & h_2\boldsymbol{u}_2 & h_3\boldsymbol{u}_3 \\ \partial/\partial v_1 & \partial/\partial v_2 & \partial/\partial v_3 \\ h_1 A_1 & h_2 A_2 & h_3 A_3 \end{vmatrix} \tag{B.3}$$

where $\boldsymbol{u}_i$, $i = 1, 2, 3$ are the unit vectors along the coordinate lines v_i and directed toward increasing v_i.

Equation (B.3) can be expanded as

$$\nabla \times \boldsymbol{A} = \frac{1}{h_2 h_3}\left[\frac{\partial(h_3 A_3)}{\partial v_2} - \frac{\partial(h_2 A_2)}{\partial v_3}\right]\boldsymbol{u}_1 + \frac{1}{h_3 h_1}\left[\frac{\partial(h_1 A_1)}{\partial v_3} - \frac{\partial(h_3 A_3)}{\partial v_1}\right]\boldsymbol{u}_2 + \frac{1}{h_1 h_2}\left[\frac{\partial(h_2 A_2)}{\partial v_1} - \frac{\partial(h_1 A_1)}{\partial v_3}\right]\boldsymbol{u}_3 \tag{B.4}$$

In prolate spheroidal coordinates (η, ξ, φ) [see (3.2)], assuming that $\boldsymbol{A}$ has only a φ-component, which is independent of φ, (B.4) can be simplified into the form

$$\nabla \times \boldsymbol{A} = \frac{1}{c(\xi^2 - \eta^2)^{1/2}}\frac{\partial}{\partial \xi}\left[(\xi^2 - 1)^{1/2} A\right]\boldsymbol{u}_\eta - \frac{1}{c(\xi^2 - \eta^2)^{1/2}}\frac{\partial}{\partial \eta}\left[(1 - \eta^2)^{1/2} A\right]\boldsymbol{u}_\xi \tag{B.5}$$

Similarly, taking the curl in (B.5) yields

$$\nabla \times \nabla \times \boldsymbol{A} = \frac{1}{c^2(\xi^2 - \eta^2)}\left\{(1 - \eta^2)^{1/2}\frac{\partial^2}{\partial \eta^2}\left[(1 - \eta^2)^{1/2} A\right] + (\xi^2 - 1)^{1/2}\frac{\partial^2}{\partial \xi^2}\left[(\xi^2 - 1)^{1/2} A\right]\right\}\boldsymbol{u}_\varphi \tag{B.6}$$

The vector Laplacian $\nabla^2 \boldsymbol{A} = 0$, is obtained from (B.2) with (B.6) in the form

$$\frac{1}{c^2(\xi^2 - \eta^2)}\left\{(1 - \eta^2)^{1/2}\frac{\partial^2}{\partial \eta^2}\left[(1 - \eta^2)^{1/2} A\right] + (\xi^2 - 1)^{1/2}\frac{\partial^2}{\partial \xi^2}\left[(\xi^2 - 1)^{1/2} A\right]\right\} = 0 \tag{B.7}$$

The corresponding expression in spherical coordinates (r, θ) can be obtained from (B.7) by performing the transformation

$c \to 0, \qquad \xi \to \infty, \qquad \eta \to cos\theta, \qquad c\xi \to r$

Thus in spherical coordinates A satisfies the equation

$$r\frac{\partial^2}{\partial r^2}(rA) + \frac{\partial}{\partial \theta}\left[\frac{1}{sin\theta}\frac{\partial}{\partial \theta}(sin\theta A)\right] = 0 \tag{B.8}$$

i.e.,

$$\frac{\partial^2}{\partial r^2}(rA) + \frac{1}{rsin\theta}\frac{\partial}{\partial \theta}\left(sin\theta\frac{\partial}{\partial \theta}A\right) - \frac{A}{rsin^2\theta} = 0 \tag{B.9}$$

Appendix C

Legendre Functions

Solution of Legendre's Equation

The Legendre equation is

$$\frac{d}{d\mu}\left[(1-\mu^2)\frac{d\Theta_n}{d\mu}\right] + n(n+1)\Theta_n = 0 \tag{C.1}$$

and its general solution can be written in the form[8]

$$\Theta_n = AP_n(\mu) + BQ_n(\mu) \tag{C.2}$$

where $P_n(\mu)$ and $Q_n(\mu)$ are called Legendre functions of the first kind and the second kind, respectively, and A and B are constants of intagration.

The associated Legendre equation is

$$\frac{d}{d\mu}\left[(1-\mu^2)\frac{d\Theta}{d\mu}\right] + \left[n(n+1) - \frac{m^2}{1-\mu^2}\right]\Theta = 0 \tag{C.3}$$

and its general solution is[8].

$$\Theta = A'P_n^m(\mu) + B'Q_n^m(\mu) \tag{C.4}$$

where $P_n^m(\mu)$ and $Q_n^m(\mu)$ are called associated Legendre functions of the first and the second

kind, respectively, and A' and B' are constants. When $-1 \leq \mu \leq +1$, $P_n^m(\mu)$ and $Q_n^m(\mu)$ are defined by[8]

$$\begin{aligned} P_n^m(\mu) &= (1-\mu^2)^{\frac{1}{2}m}\frac{d^m P_n(\mu)}{d\mu^m} \\ Q_n^m(\mu) &= (1-\mu^2)^{\frac{1}{2}m}\frac{d^m Q_n(\mu)}{d\mu^m} \end{aligned} \tag{C.5}$$

For $-1 \leq \mu \leq +1$, Hobson[8] has introduced the factor $(-1)^m$ to the right hand side of the above equations. For an unrestricted domain of the argument, the associated Legendre functions are defined by[15]

$$\begin{aligned} P_n^m(z) &= (1-z^2)^{\frac{1}{2}m}\frac{d^m P_n(z)}{dz^m} \\ Q_n^m(z) &= (1-z^2)^{\frac{1}{2}m}\frac{d^m Q_n(z)}{dz^m} \end{aligned} \tag{C.6}$$

Some Useful Properties of Legendre Functions[1]

$$\begin{aligned} \frac{d}{d\eta}\left[(1-\eta^2)^{1/2}P_n^1(\eta)\right] &= n(n+1)P_n(\eta) \\ \frac{d}{d\xi}\left[(\xi^2-1)^{1/2}P_n^1(\xi)\right] &= n(n+1)P_n(\xi) \\ \frac{d}{d\xi}\left[(\xi^2-1)^{1/2}Q_n^1(\xi)\right] &= n(n+1)Q_n(\xi) \end{aligned} \tag{C.7}$$

$$Q_n^1(\xi)\frac{dP_n^1(\xi)}{d\xi} - P_n^1(\xi)\frac{dQ_n^1(\xi)}{d\xi} = \frac{-n(n+1)}{\xi^2-1} \tag{C.8}$$

$$\begin{aligned} (1-\eta^2)P_n(\eta) &= -\frac{1}{n}\left[\eta P_n^1(\eta) - P_{n-1}^1(\eta)\right] \\ (\xi^2-1)Q_n(\xi) &= -\frac{1}{n}\left[\xi Q_n^1(\xi) - Q_{n-1}^1(\xi)\right] \end{aligned} \tag{C.9}$$

Orthogonality property[8]

$$\begin{aligned}\int_{-1}^{+1} P_n^m(x)P_l^m(x)dx =& \frac{2}{2n+1}\frac{(n+m)!}{(n-m)!}\delta_{nl} \; for \; x \in [-1,+1] \\ n =& 0,1,2,3,..... \\ m =& 0,\pm 1,\pm 2,....., \pm n \\ \delta_{nl} =& \begin{cases} 0 & \text{if } l \neq n, \\ 1 & \text{if } l = n. \end{cases}\end{aligned} \tag{C.10}$$

$$\begin{aligned} P_n^1(\infty) \to \infty, \qquad & Q_n^1(\pm 1) \to \infty \\ P_n(-1) \to \infty, \quad & when \; n \neq integer \end{aligned} \tag{C.11}$$

Asymptotic Expansions of Associated Legendre Functions with Large Arguments [1]

$$\begin{aligned} P_n^m(z) &\underset{|z|\to\infty}{\longrightarrow} \frac{(2n)!}{2^n n!(n-m)!}z^n \\ Q_n^m(z) &\underset{|z|\to\infty}{\longrightarrow} -\frac{(n)!(n+m)!2^n}{(2n+1)!z^{n+1}} \end{aligned} \tag{C.12}$$

Recurrence Relations

For real or complex arguments[14]

$$(n-m+1)P_{n+1}^m(z) = (2n+1)zP_n^m(z) - (n+m)P_{n-1}^m(z) \tag{C.13}$$

Appendix D

Modified Bessel Functions

Solution of the Modified Bessel Equation

Let us consider the differential equation

$$\frac{d^2R}{dv^2} + \frac{1}{v}\frac{dR}{dv} - \left(1 + \frac{n^2}{v^2}\right) R = 0 \tag{D.1}$$

which known as the modified Bessel equation and whose solution can be expressed in terms of modified Bessel functions of the first kind $I_n(v)$ and the second kind $K_n(v)$ [8].

$$R_n(v) = \alpha I_n(v) + \beta K_n(v) \tag{D.2}$$

where α and β are constants. The spherical Bessel functions $j_n(v)$ and $k_n(v)$ are defined in terms of the modified Bessel functions $I_{n+\frac{1}{2}}$ and $K_{n+\frac{1}{2}}$,

$$\begin{aligned} j_n(v) &\equiv \sqrt{\frac{\pi}{2v}} I_{n+\frac{1}{2}}(v) \\ k_n(v) &\equiv \sqrt{\frac{\pi}{2v}} K_{n+\frac{1}{2}}(v) \end{aligned} \tag{D.3}$$

Series Expansions for Modified Bessel Functions With Small Arguments [8]

$$\begin{aligned} I_{n+\frac{1}{2}}(\upsilon) &\underset{\upsilon \to 0}{\longrightarrow} \sqrt{\frac{2\upsilon}{\pi}} \frac{\upsilon^n}{(2n+1)!!} \\ K_{n+\frac{1}{2}}(\upsilon) &\underset{\upsilon \to 0}{\longrightarrow} \sqrt{\frac{\pi}{2\upsilon}} \frac{(2n-1)!!}{\upsilon^n} \end{aligned} \tag{D.4}$$

A Useful Property of Modified Bessel Functions[8]

$$I_n'(x) = I_{n-1}(x) - \frac{n}{x} I_n(x) \tag{D.5}$$

Appendix E

Principal Curvatures for Prolate and Oblate Spheroids

Let's consider a spheroid as shown in the Fig.E.1

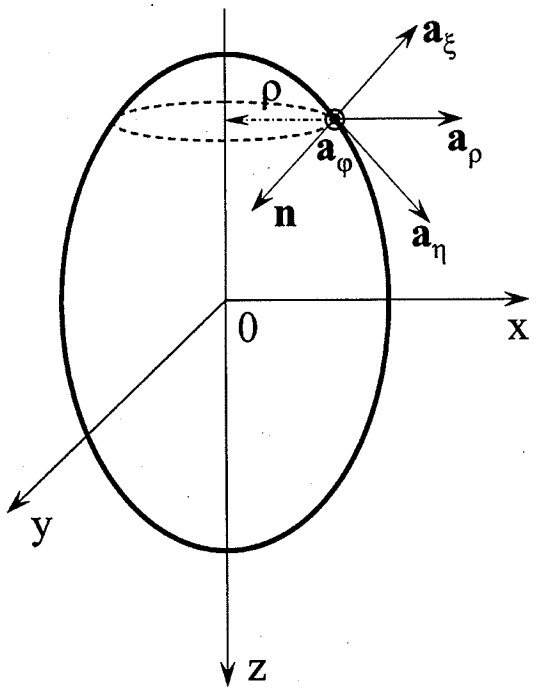

Figure E.1: Principal curvature directions for a spheroid.

Let's assume the x-axis to be the reference axis. The spheroid is generated by the revolution of the ellipse in the $x - z$ plane about the z-axis. The principal curvatures at a point on the surface are defined as the maximum and the minimum normal curvatures at the point considered and are denoted by K_u and K_v, $K_u = 1/R_u$ and $K_v = 1/R_v$, where R_u and

R_v are the radii of the principal curvatures. The lines of curvature at a point on a surface are defined as the lines along which the normal curvatures of the surface attain extremal values[12]. The lines of curvature of a surface of revolution are it's meridians and parallels[12].

For the spheroid shown in Fig. E.1 the lines of curvature are the ellipses in plane determined by the z-axis and the circles with constants ξ_0 and η (hence constant z). From (3.1), the equation of such a circle for a prolate spheroid is

$$x^2 + y^2 = c^2(1 - \eta^2)(\xi_0^2 - 1) \tag{E.1}$$

The radius of curvature of the circle in (E.1) at $\varphi = 0$ (i.e. $y = 0$) is

$$\rho = c\sqrt{(1 - \eta^2)(\xi_0^2 - 1)} \tag{E.2}$$

Hence the principal curvature K_φ can be expressed as

$$K_\varphi = \frac{1}{\rho}\boldsymbol{a}_\rho \cdot \boldsymbol{a}_\xi \tag{E.3}$$

Substituting ρ from (E.2) and $\boldsymbol{a}_\rho \cdot \boldsymbol{a}_\xi$ from (4.27) we get

$$K_\varphi = \frac{\xi_0}{c\sqrt{(\xi_0^2 - 1)(\xi_0^2 - \eta^2)}} \tag{E.4}$$

The equation of the meridian of a prolate spheroid(i.e. the ellipse in the $x - z$ plane) is determined from (3.1) with $\varphi = 0$, for example, in the form

$$\frac{x^2}{(\xi_0^2 - 1)} + \frac{z^2}{\xi_0^2} = c^2 \tag{E.5}$$

For a plane curve given by the equation $x = x(z)$, the curvature is expressed as[13]

$$K_1 = \frac{x''}{(1+(x')^2)^{3/2}} \tag{E.6}$$

where x' and x'' are the first and second derivative of x with respect to z, respectively. From (E.5) and (E.6) the principal curvature K_η is derived in the form

$$K_\eta = \frac{\xi_0}{c}\frac{(\xi_0^2-1)^{1/2}}{(\xi_0^2-\eta^2)^{3/2}} \tag{E.7}$$

For an oblate spheroid, the two principal curvatures are obtained in the form

$$K_\varphi = \frac{1}{c\sqrt{(\xi_0^2+1)(\xi_0^2+\eta^2)}} \tag{E.8}$$

$$K_\eta = \frac{\xi_0}{c}\frac{(\xi_0^2+1)^{1/2}}{(\xi_0^2+\eta^2)^{3/2}} \tag{E.9}$$

Note

In the case of a sphere, all the curves at any point on the sphere can be taken as principal curvature curves since the principal directions are undetermined [12].

Appendix F

Exact Analytical Solution for a Conducting Sphere in the Presence of a Current-Carrying Circular Turn

Magnetic Vector Potential External to the Sphere

For the inducing system shown in Fig. 2.1, the resultant magnetic vector potential external to the conducting spheroid is obtained by the method of separation of variables as given in (2.16), such that

$$A_{ext} = \sum_{n=1}^{\infty} C_n r^{-(n+1)} P_n^1(cos\theta) + \frac{\mu_0 I_s}{2} sin\theta_s r_s \sum_{n=1}^{\infty} \frac{1}{n(n+1)} \left(\frac{r_<^n}{r_>^{n+1}} \right)^n P_n^1(cos\theta_s) P_n^1(cos\theta) \tag{F.1}$$

Magnetic Vector Potential Inside the Sphere

The magnetic vector potential internal to the conducting sphere has only a component in the direction of the inducing current and satisfies the equations

$$\nabla^2 \boldsymbol{A}_{in} - k^2 \boldsymbol{A}_{in} = 0 \qquad for \;\; 0 \leq r \leq r_0 \tag{F.2}$$

$$\nabla \cdot \boldsymbol{A}_{in} = 0 \tag{F.3}$$

where $k^2 = j\omega\mu\sigma$. Equation (F.2) can be expressed as

$$\frac{\partial^2}{\partial r^2}(rA_{in}) + \frac{1}{rsin\theta}\frac{\partial}{\partial\theta}\left(sin\theta\frac{\partial}{\partial\theta}A_{in}\right) - \frac{A_{in}}{r^2sin\theta} - k^2A_{in} = 0 \tag{F.4}$$

Let us assume that the solution of (F.4) can be expressed as $A_{in} = L(r)M(\theta)r^{-1/2}$ [8]. Substituting in (F.4), denoting $x \equiv cos\theta$, and dividing by $r^{-1/2}LM$ yields

$$\frac{r^2}{L}\left[\frac{d^2L}{dr^2} + \frac{1}{r}\frac{dL}{dr} - \frac{L}{4r^2}\right] - k^2r^2 + \frac{1}{M}\frac{d}{dx}\left[(1-x^2)\frac{dM}{dx}\right] - \frac{1}{1-x^2} = 0 \tag{F.5}$$

with $\frac{1}{M}\frac{d}{dx}\left[(1-x^2)\frac{dM}{dx}\right] - \frac{1}{1-x^2} = -n(n+1)$, we have

$$\frac{d}{dx}\left[(1-x^2)\frac{dM}{dx}\right] + \left[n(n+1) - \frac{1}{1-x^2}\right]M = 0 \tag{F.6}$$

The solution of (F.6) is expressed in terms of associated Legendre functions in the form

$$M(\theta) = \lambda_n P_n^1(x) + \psi_n Q_n^1(x) \tag{F.7}$$

where λ_n and ψ_n are constants. From (F.5), L satisfies the equation

$$\frac{d^2L}{d(kr)^2} + \frac{1}{kr}\frac{dL}{d(kr)} - \left[1 + \frac{(n+1/2)^2}{(kr)^2}\right]L = 0 \tag{F.8}$$

This equation is in the form of the modified Bessel equation as given in (D.1) in Appendix D and its solution can be expressed in terms of modified Bessel functions first kind $I_{n+\frac{1}{2}}$ and the second kind $K_{n+\frac{1}{2}}$,

$$L(kr) = \lambda_n' I_{n+\frac{1}{2}}(kr) + \psi_n' K_{n+\frac{1}{2}}(kr) \tag{F.9}$$

where λ'_n and ψ'_n are constants of integration. By taking in to account the properties of the associated Legendre functions as given in (C.11) and the properties of the modified Bessel functions as given in (D.4), and imposing the condition that $\boldsymbol{A}_{in}$ be finite everywhere inside the conductor, the solution for the magnetic vector potential internal to the conducting sphere is expressed as

$$A_{in} = r^{-1/2} \sum_{n=1}^{\infty} D_n P_n^1(cos\theta) I_{n+\frac{1}{2}}(kr) \tag{F.10}$$

where D_n are constants to be determined.

Determination of the Integration Constants

The constants of integration in (F.1) and (F.10) can be determined by imposing the continuity of the tangential components of the electric and magnetic field intensities E_φ and H_θ, respectively, at the conductor surface, which are given by (2.20) and (2.21) respectively. Assuming that the permeability of the conductor is the same as that of the free space, the following relations are to be satisfied,

$$\begin{aligned} A_{in}\Big|_{r=r_0} &= A_{ext}\Big|_{r=r_0} \\ \frac{\partial}{\partial r}(rA_{in})\Big|_{r=r_0} &= \frac{\partial}{\partial r}(rA_{ext})\Big|_{r=r_0} \end{aligned} \tag{F.11}$$

These equations yield[9][10]

$$\begin{aligned} C_n =& \frac{\mu_0 I_s}{2} \frac{sin\theta_s}{n(n+1)} \frac{r_0^{2n+1}}{r_s^n} \left[\frac{(2n+1)}{kr_0} \frac{I_{n+\frac{1}{2}}(kr_0)}{I_{n-\frac{1}{2}}(kr_0)} - 1 \right] P_n^1(cos\theta_s) \\ D_n =& \frac{\mu_0 I_s}{2} \frac{sin\theta_s}{kr_0^{1/2}} \frac{2n+1}{n(n+1)} \left(\frac{r_0}{r_s}\right)^n \frac{P_n^1(cos\theta_s)}{I_{n-\frac{1}{2}}(kr_0)} \end{aligned} \tag{F.12}$$

Substituting C_n and D_n in (F.1) and (F.10), the magnetic vector potentials internal and external to the conducting sphere are derived in the form

$$A_{in} = \frac{\mu_0 I_s}{2} \frac{sin\theta_s}{kr_0^{1/2}} r^{-1/2} \sum_{n=1}^{\infty} \frac{2n+1}{n(n+1)} \left(\frac{r_0}{r_s}\right)^n \frac{j_n(kr)}{j_{n-1}(kr_0)} P_n^1(cos\theta_s) P_n^1(cos\theta) \tag{F.13}$$

$$A_{ext} = \frac{\mu_0 I_s sin\theta_s}{2} \sum_{n=1}^{\infty} \left\{ \left(\frac{r}{r_s}\right)^n + \frac{r_0^{2n+1}}{r_s^n r^{n+1}} \left[\frac{(2n+1)}{kr_0} \frac{j_n(kr_0)}{j_{n-1}(kr_0)} - 1 \right] \right\} \cdot \frac{P_n^1(cos\theta_s) P_n^1(cos\theta)}{n(n+1)} \tag{F.14}$$

where j_n denotes spherical Bessel functions of the first kind as defined in (D.3). The resultant magnetic vector potential produced by an inducing system having N_t turns can be determined by superposing the magnetic vector potentials produced by the individual turns.

Appendix G

Surface Impedance with First Order Curvature Correction

The surface impedance of a good conductor with the first order curvature correction Z_s' can be obtained from (3.58) in the form

$$Z_s' = (1-p)Z_s \tag{G.1}$$

where Z_s is the standard surface impedance derived on the basis of the exact field solution for a conducting semi-space as given in (A.15), and $p = \frac{1}{4}(1+j)\delta K_d$, where K_d is the difference between the two principal curvatures and δ is the skin depth as given in (A.16). By substituting for Z_s and p in (G.1) we get

$$Z_s' = R_s\left[1 - j\left(1 - \frac{\delta K_d}{2}\right)\right] \tag{G.2}$$

Thus the real part of Z_s' is the same as that of Z_s.

Bibliography

[1] I.R. Ciric, "Electromagnetic levitation in axially symmetric systems," *Rev. Roum. Sci. Electotech. et Energ.*, Vol. 15, pp. 35-73, 1970.

[2] T.B. Senior and J.L. Volakis, *Approximate Boundary Conditions in Electromagnetics*, IEE electromagnetic waves series 41, The Institution of Electrical Engineers, London, United Kindom, pp. 7-12, 1995.

[3] T.B.A. Senior, "Impedance boundary conditions for imperfectly conducting surfaces," *Appl. Sci. Res.*, section B., vol.8, pp.418-436, 1960.

[4] S.A. Schelkunoff, "The electromagnetic theory of coaxial transmission lines and cylindrical shields," *The Bell System Technical Jounal.*, vol.08, pp.532-579, 1934.

[5] T.H. Fawzi, M. Taher Ahmed and P.E. Burks, "On the use of the impedance boundary conditions in eddy current problems, " *IEEE. Trans.Magn.*, vol.21, pp.1835-1840, Sept 1985.

[6] K.M. Mitzner, "An integral equation approach to scatering from a body of finite conductivity," *Radio Science.*, vol.2(New Series), No.12, pp. 1459-1470, December 1967.

[7] J.D. Jackson, *Classical Electrodynamics*, 3rd ed. John Wiley & Sons,Inc., pp. 218-220, 1999.

[8] W.R. Smythe, *Static and Dynamic Electricity*, 3rd ed. McGraw-Hill,Inc., pp. 152-208, 1968.

[9] A. Tugulea and I.R. Ciric, "Electromagnetic field of current-carrying circular turns in the presence of conducting spherical shells," *St. cerc. energ. electr.*, vol.18, 2, pp. 355-379, 1968.

[10] W. Brisley and B.S. Thornton,"Electromagnetic levitation calculations for axially symmetric systems," *Brit. J. Appl. Phys.*, vol.14, pp. 682-686, 1963.

[11] S.Morse and J. Feshbach, *Methods of Theoretycal Physics*, vol.1, McGraw-Hill,Inc., pp. 655-666, 1953.

[12] D.J. Struik, *Lectures on Classical Differential Geometry*, 2nd Ed, Addison-Wesley publishing company, Inc., Reading, Massachusetts, U.S.A., London, England, pp. 80-87, 1961.

[13] A.V. Pogorelow, *Differential Geometry*, P.Noordhoff N.V., Groningen, The Netherlands, pp. 49-52, 1988.

[14] M. Abramowitz and I.A. Stegun, *Hand book of Mathematical Functions with Formulas, Graphs, and Mathematical Tables*, National Bureau of Standards, Applied Mathematics Series. 55, U.S. Government printing office, washington,D.C.,20402, pp. 332-353, June 1964.

[15] S.Zhang and J. Jin, *Computation of Special Functions*. John Wiley & Sons,Inc., pp. 77-125, 1996.

[16] W. Gautshi, Alorithm 259, Legendre functions for arguments larger than one, Prude University Lafayette, Ind. and Argonne National Laboratory, Argone, III. [Online]. Available: http://portal.acm.org/portal.cfm

[17] S. Zhang and J. Jin, MATLAB routines for computation of special functions. [Online]. Available: http://ceta.mit.edu/comp_spec_func/